

**Characterization of the effects of climate
variation on land surface temperature and soil
moisture through stochastic analysis of long
term SSM/I observations over the Tibetan
plateau**

Ofwono Matthew
February, 2010

Characterization of the effects of climate variation on land surface temperature and soil moisture through stochastic analysis of long term SSM/I observations over the Tibetan plateau

by

Ofwono Matthew

Thesis submitted to the International Institute for Geo-information Science and Earth Observation, in partial fulfilment of the requirements for the degree of Master of Science in Geo-information Science and Earth Observation, Specialisation: Surface Hydrology

Thesis Assessment Board

Chairman:	Prof. Dr. Bob Su	WRS Depart' ITC - University of Twente
External examiner:	Dr. Richard de Jeu	Vrije Universiteit Amsterdam
Supervisor 1:	Rogier Van der Velde	WRS Depart' ITC - University of Twente
Supervisor 2:	Dr. Suhyb Salama	WRS Depart' ITC - University of Twente
Adviser:	Lei Zhong	WRS Depart' ITC - University of Twente



**INTERNATIONAL INSTITUTE FOR GEO-INFORMATION SCIENCE AND EARTH OBSERVATION
ENSCHEDA, THE NETHERLANDS**

Disclaimer

This document describes work undertaken as part of a programme of study at the International Institute for Geo-information Science and Earth Observation. All views and opinions expressed therein remain the sole responsibility of the author, and do not necessarily represent those of the Institute.

Abstract

This study evaluates the temporal and spatial variability in land surface temperature (LST) and soil moisture over the Tibetan Plateau (TP) in the past 2 decades (1988-2008). The LST and soil moisture time series were derived from brightness temperatures (T_B) measured by the Special Sensor Microwave Imager (SSM/I). The retrieval is based on the τ - ω model, whereby the horizontally (H) and vertically (V) polarized 19 GHz T_B are utilized for the simultaneous inversion of soil moisture and the transmissivity. Within this retrieval approach, the temperature of the emitting layer is estimated using the V-polarized 37 GHz channel. The comparison of the retrievals against a time series of LST and soil moisture measured over a period of 4-years gives an error of ± 2.87 K and ± 0.040 m³m⁻³ respectively. The western part of the TP is significantly colder than the eastern part due to a large elevation difference. The temporal variation of soil moisture over the TP follows the monsoon sequence. From November to March the soil moisture is almost zero. However as the monsoon season arrives in April the moisture content begins to rise reaching its maximum value by July and dissipates by October. Spatially, soil moisture is highest in the south and eastern parts of the TP. Image trend analysis revealed that, the entire TP experienced significant warming over the last two decades except the water bodies. However, the central TP experienced more significant positive trend in LST anomalies. A similar trend is observed over scattered areas in the east and northern part of TP, while the south and south eastern part of the TP experienced the least changes in temperature anomalies. The magnitude of warming over the TP is in the range of 0.2°C to 1.1°C/decade. Warming was more paramount at elevations over 3000m above sea level compared to areas with elevation below 3000m above sea level. The western and northern part of the TP experienced an increasing significant trend in mean annual soil moisture anomalies. While the eastern and south eastern part of the TP showed no trend in soil moisture anomalies. The soil moisture anomalies over the TP increased at the rate of 0.03 to 0.13% (volume/volume) per year. The annual trend was highest during the summer monsoon season than during the winter season.

Acknowledgements

This thesis wouldn't have been possible without the dedicated support of my supervisors. First, my sincere appreciation goes to Rogier Van der Velde, my primary supervisor, for being an extraordinary mentor throughout the research period. Rogier not only gave me the necessary support and advice but also up scaled my programming capability which was an absolute necessity for this research and helped me trouble shoot difficulties that I came across in a short notice. And most importantly it was always a great pleasure to work with Rogier, his door was always open to discuss my results and I always walked out with relevant literature. I hope to continue working with him in the future.

Secondly, I would like to thank my second Supervisor Dr. Suhyb Salam. Suhyb is very a warm hearted person and great to work with. I sincerely appreciate Suhyb's support, and especially his rigorous editing which made me improve on my writing skills. I also thank Suhyb for mentoring me on paper writing skills.

I am grateful to the Erasmus Mundus Lot 10 programme of the European Union, without their financial support, I would never have been to ITC in the first place. I would like to say thank you to my student advisor Lei Zhong and my colleagues who were patient enough with me when I "hijacked" five computers for nearly two months. I surely had to use those computers in order to complete my thesis within the stipulated time frame and I am sorry for any inconveniences that I could have caused to other students.

Table of contents

1. Introduction.....	1
1.1. Background.....	1
1.2. Problem statement.....	1
1.3. General Objective.....	2
1.3.1. Specific Objectives.....	2
1.4. Research questions:	2
1.5. Hypothesis.....	2
1.6. Outputs.....	2
1.7. Thesis structure	3
2. Literature review	5
2.1. Global climate change	5
2.2. Remote sensing of land surface variables.....	5
2.2.1. Soil moisture and land surface temperature retrieval from passive microwave radiometers	6
2.3. Trend analysis of time series.....	6
3. Study area and data set.....	9
3.1. Description of the study area	9
3.2. SSM/I Data set.....	9
3.3. Measured land surface data.....	10
4. LST and soil moisture retrieval methods	11
4.1. Passive Microwave theory.....	11
4.2. Dielectric constant and soil moisture.....	11
4.3. Relationship between brightness temperature at 37GHz and LST	12
4.4. Retrieval of land surface temperature, Soil moisture and vegetation transmissivity.....	13
4.4.1. Soil moisture retrieval algorithm.....	13
4.4.2. Topp model.....	14
4.4.3. Vegetation effect on emissivity.....	14
4.4.4. Effect of surface roughness on emissivity	15
4.4.5. Retrieval of soil moisture from frozen soils	19
4.4.6. Effect of single scattering albedo on soil moisture retrieval.....	20
5. Results and discussions.....	23

6. Evaluation of trend in the soil moisture and LST time series	27
7. Uncertainty and sensitivity analysis.....	33
7.1. Derivation of uncertainty matrix	33
7.2. Results and discussions	36
8. Time series analysis (TSA)	39
8.1. Theory.....	39
8.2. Model selection	39
8.3. Model estimation (fitting)	50
8.4. Model verification (validation)	51
9. Summary and Conclusions	55
10. References:	57

List of figures

Figure 1: Digital elevation model of the Tibetan Plateau overlaid with locations of ARIMA model and Error analysis.....	9
Figure 2: LST versus 37GHz vertical polarization brightness temperature	12
Figure 3: Normal probability plot of the residuals of LST vs 37GHz v.pol brightness temperature	13
Figure 4: Schematic diagram of LST, soil moisture and vegetation transmissivity retrieval.....	17
Figure 5: Influence of different values of surface roughness on retrieved soil moisture	18
Figure 6: Effect of freezing on soil moisture retrieval (Naqu station 2006 data).....	19
Figure 7: Calibration of soil moisture retrieval from a frozen soil (Naqu station 2006 data)	20
Figure 8: Effect of single scattering albedo on soil moisture retrieval (Naqu station 2006 data)	21
Figure 9: comparison between measured LST and retrieved LST	23
Figure 10: comparison between retrieved soil moisture and measured soil moisture.....	23
Figure 11: Retrieved vegetation transmissivity.....	24
Figure 12: Histogram of LST retrieval error (A) and soil moisture retrieval error (B).....	25
Figure 13: Spatial soil moisture (A) and LST (B) distribution over the Tibetan plateau (July 2004)...	26
Figure 14: Trend in annual mean soil moisture anomalies (A) and corresponding t-Statistics (B)	27
Figure 15: 21 year monthly mean soil moisture trend over the central TP	28
Figure 16: Trend in mean monthly soil moisture during the monsoon season.....	29
Figure 17: Normalized soil moisture anomaly magnitudes during the monsoon season	30
Figure 18: Trend in mean annual LST anomalies (A) and corresponding t-Statistics (B).....	31
Figure 19: Comparison between warming during February and June.....	32
Figure 20: Schematic illustration of ARIMA modelling of soil moisture and LST.....	41
Figure 21: Decomposed soil moisture ($m^3 m^{-3}$) [A] and LST(k) [B]	42
Figure 22: Land surface temperature residuals after eliminating periodicity (location 12)	44
Figure 23: soil moisture residuals after eliminating periodicity (location 16)	45
Figure 24: Land surface temperature residuals after removing both periodicity and trend (location 12)	46
Figure 25: soil moisture residuals after removing both periodicity and trend (location 16).....	46
Figure 26: ACF and PACF plots demonstrating a clear AR process of LST at location 12	48
Figure 27: ACF and PACF plots demonstrating a case of a MA and AR process of soil moisture at location 16. Note; the dotted blue line represents the 95% confidence limits.....	49
Figure 28: ACF plot of fitted LST residuals	51
Figure 29: ACF plot of fitted soil moisture residuals.....	52

Figure 30: Long term forecasting of soil moisture at location 16 52
Figure 31: long term forecasting of Land surface temperature at location 12..... 53

List of tables

Table 1: Basic characteristics of SSM/I	10
Table 2: Regression analysis of LST versus 37GHz v Pol. Brightness temperature.....	12
Table 3: Magnitude of errors caused by a 1% uncertainty in the input variables of LST, soil moisture and vegetation transmissivity retrieval.....	36
Table 4: Relative contribution of input variables to the total standard deviation of LST, soil moisture and vegetation transmissivity	36
Table 5: Summary of LST periodic function at location 12.....	44
Table 6: Summary of soil moisture periodic function at location 16.....	45
Table 7: ARIMA models for LST and soil moisture derived from the analysis of ACF and PACF	47
Table 8: Comparison of suitable ARIMA models for soil moisture	50
Table 9: comparison of suitable ARIMA models for LST	50
Table 10: Summary of soil moisture and LST forecasting accuracy	53

1. Introduction

1.1. Background

Climate variability is one of the major global concerns due to its potential impact on socio-economic and political stability of the world. Understanding the changes and characterizing the natural variability of the global climate system has drawn the attention of the scientific community in the past few decades. Climate change indicators are physical variables that are strongly influenced by climatic conditions, such as land surface temperature and soil moisture (Latifovic and Pouliot 2007; Löscher, Retscher et al. 2008).

Land surface temperature (LST) and soil moisture are important factors in global change studies, energy balance, spatial and temporal dynamics of vegetation and have a role in controlling feedback mechanism of climate (Tan 2007; Raynolds, Comiso et al. 2008; Alec Sithole 2009). A change in soil moisture results in a change in the partitioning of net radiation into sensible heat flux and latent heat causing either a cooling or warming of the atmosphere. Soil moisture also influences runoff and is a limiting factor for plant growth.

Available data for the analysis of climate change studies are, in general, scarce and consist of point scale observations or simulated data. However, remote sensing plays a critical role in climate change studies by providing a synoptic information on the Earth's environment at higher time frequency.

Numerous studies on climate variability, carried out over the past decade involved the use of climate proxies such as plant phenology, especially normalized difference vegetation index (NDVI) (Krishna Prasad, Badarinath et al. 2007; Nagai, Ichii et al. 2007; Tao, Yokozawa et al. 2008), derived from visible spectral bands. The visible part of the solar spectrum is, however, affected by atmospheric absorption and aerosol scattering, which require reliable atmospheric correction procedure. The use of microwave remote sensing overcomes this limitation of the visible band. Microwaves are longer and are able to penetrate clouds. Moreover, at these longer wavelengths emission is not only determined by the LST, but also the soil moisture content. Both land surface states are strongly affected by weather and can be used as indicators for climate change.

1.2. Problem statement

The effect of climate change will be most notable in vulnerable environments. One of such region is the Tibetan Plateau. The vast Tibetan landscape covers an area the size of Western Europe at an altitude of more than 4000 m above sea level. This huge obstacle in the centre of Asia has an important effect on guiding the high altitude jet streams over Asia and, as such, influences large scale weather systems (e.g. Asian Monsoon). The anomalies of surface heating over the Tibetan Plateau (TP), therefore, greatly influence atmospheric circulation in China, East Asia (EA) and even the Northern Hemisphere. The anomalies of surface heating field over TP might cause the abnormal atmospheric circulation in EA. Thus, it has great influences on the climate in China, especially the anomalies of summer precipitation in China. However, this investigation of the influence of climate

variation on land surface variables such as LST and soil moisture over the TP has received little attention.

1.3. General Objective

The general objective of this study is to evaluate the effects of possible climate variations on land surface temperature and soil moisture over the Tibetan plateau, using data retrieved from special sensor microwave imager (SSM/I) and stochastic methods

1.3.1. Specific Objectives

The specific objectives of the study are;

- To retrieve land surface temperature and soil moisture of the study area from SSM/I;
- To evaluate the temporal variability of land surface temperature and soil moisture;
- To apply a stochastic method to identify the effects of climate variation on the retrieved soil moisture and LST.

1.4. Research questions:

- Are there any differences in the mean annual LST and soil moisture at 5% level of significance?
- What is the trend in LST and soil moisture over the TP over the last 20 years?
- What is (are) the parameter(s) and the order of the Auto Regressive Integrated Moving Average (ARIMA) model which describes the temporal LST and soil moisture variability over the TP?

1.5. Hypothesis

- The mean annual land surface temperature and the soil moisture between distinct years are statistically different at 95% confidence level;
- There is a statistically significant positive trend (increase) in land surface temperature and soil moisture over time;
- Both land surface temperature and soil moisture over the TP can be represented by ARIMA model of the same order for the entire area.

1.6. Outputs

- Mean LST and soil moisture time series maps;
- Time series plots of LST and soil moisture;
- Autocorrelation function (ACF) and partial autocorrelation function (PACF) plots of LST and soil moisture;
- ARIMA models for LST and soil moisture;
- Time series plots of LST and soil moisture residuals;
- Predicted LST and soil moisture time series.

1.7. Thesis structure

Chapter 1 provides a general introduction, problem statement, objectives, research questions, research outputs and a descriptive outline. Chapter 2 provides literature review on what has been done on climate change studies, soil moisture and LST retrievals and time series analysis. The study area and data set used in this study is described in chapter 3 while the methodologies and the theory behind the LST and soil moisture retrieval are explained in chapter 4. The results and discussions of LST and soil moisture retrieval are outlined in chapter 5. Chapter 6 evaluates the trend in LST and soil moisture time series. Chapter 7 discusses uncertainty and sensitivity analysis of the retrieval algorithm. Chapter 8 discusses the times series analysis. 9 provide a general summary and conclusion of this study followed by a list of used references.

2. Literature review

2.1. Global climate change

The industrial revolution brought with it an increased emission of greenhouse gases (GHG). The elevated concentration of GHG's in the atmosphere enhanced the greenhouse effect resulting in an increase of 0.3 – 0.6°C in the global air temperature over the last century (Zamostny, Kukula et al. 1999; Matondo, Peter et al. 2004)

There is evidence that enhanced greenhouse effect not only increases the global air temperature, but may also have an impact on other climate variables. For example, Boyles and Raman,(2003) evaluated 49 years (1949 – 1998) of observed data (temperature and precipitation) to analyze climate variability over North Carolina using trend analysis of single point observations. The analysis revealed an increase in precipitation over the last 50 years during the winter seasons but a decrease during the summer seasons. The duration of warm season had also increased and the minimum temperature over the last 10 years of the study was higher than average minimum temperature, although it was not significantly different from the observed temperatures in the 1950s.

Based on digital elevation differences of three different dates and trend analysis of 50 years (1950 – 2000) of observed climate variables (monthly mean temperature and precipitation), Bown and Rivera, (2007) evaluated climate change and glacial behaviour over the Chilean lake district. The study found, there was a marked cooling of temperature over the study period at the lower altitude but a warming trend at higher elevation. Consequently, it was also apparent that there was glacial thinning over the study period, but the most significant finding was that the rate of thinning was 3 times faster between 1981 and 1998, leading to an annual drop rate in elevation by as much as 51m per annum. The overall change in elevation over the study period was -2.3m per year, well above the error margin of 0.6m. There was a general decrease in precipitation over the study area particularly during the last two decades of the study period.

Zhao et al. (2004) analyzed 30 years (1967 – 1997) of observed data (freezing depth, mean annual air temperature, ground surface temperature and annual precipitation) from 50 meteorological stations over the Tibetan plateau, using cluster analysis method for evidence of climate change. There was significant warming in the ground temperature than the air temperature and the warming was paramount in the warm season than in the cold season. However, considering the size of the Tibetan plateau, 50 meteorological stations are not representative of the area hence using remote sensing observations is more appropriate.

2.2. Remote sensing of land surface variables

It is almost 4 decades since the launch of Landsat-1 satellite into orbit. As such, sufficient data has been amassed to define climate normal at least in the visible and near infrared spectral domains. Also, via the special sensor microwave imager (SSM/I) on board the defence meteorological satellite program (DMSP), a time series of 21 years of observations in the microwave domain has been collected.

In comparison to wavelengths in the visible spectral domain of the electromagnetic spectrum, microwaves are less affected by atmospheric scattering, absorption by hydrometeors and can penetrate through clouds due to their long wavelengths. Moreover, microwave observations have been used in the past for the retrieval of physical quantities affected by climate variability such as LST and soil moisture.

2.2.1. Soil moisture and land surface temperature retrieval from passive microwave radiometers

Numerous algorithms have been developed for soil moisture and LST retrieval from passive microwave sensors. All these algorithms make use of the tau - omega model (Mo, Choudhury et al. 1982) for the retrieval of soil moisture and the relationship between emissivity and brightness temperature as basis for the retrieval of LST (McFarland, Miller et al. 1990; Drusch, Wood et al. 2001; Magagi and Kerr 2001; Morland, Grimes et al. 2001; Jackson, Hsu et al. 2002; Bindlish, Jackson et al. 2003; De Ridder 2003; Wen, Jackson et al. 2005; Gao, Wood et al. 2006).

Soil moisture retrieval algorithms based on the radiative transfer equation in which optical thickness is estimated from vegetation water content has been developed, for example, (Drusch, Wood et al. 2001; Jackson, Hsu et al. 2002; Bindlish, Jackson et al. 2003), used normalized difference vegetation index (NDVI) as a proxy for vegetation water content in their soil moisture retrieval algorithms.

Weng and Grody (1998) developed a land surface temperature retrieval algorithm based on the 19.35GHz and 22.2GHz SSM/I brightness temperature channels using a non linear algebra. Since the two frequencies are close to each other, variation in surface emissivity is minimized and there is a limited effect of atmospheric scattering and absorption by hydrometeors due to the relatively lower frequencies being used. Wen, Su et al (2003) used similar frequencies of TMI to retrieve land surface temperature based on the similar assumption.

2.3. Trend analysis of time series

de Beurs and Henebry (2005) proposed a frame work for the analysis of long image time series involving two steps, that is; separation of mean values between periods which they referred to as step changes and image trend analysis within periods based on Mann – Kendall trend test rather than linear regression trend analysis method. The technique was then used to analyze land use changes over Kazakhstan using NDVI

Vinnikov and Robock (2002) proposed a stochastic method to analyze trends in moments of climate indices in which observed trend in a climatic variable is deducted from the observed time series. A time series is then calculated for the resultant variables raised to different powers and a standard trend analysis is carried out for the generated time series. The method was used to analyze diurnal and seasonal surface air temperature (48 years of data 1951 -1999) from 9 meteorological stations distributed over the United States (Vinnikov, Robock et al. 2002)

Piwowar and Ledrew (2002) used an automated ARIMA process to analyze 9 years of sea ice concentration data, derived from scanning multichannel microwave radiometer (SMR) while, Romilly (2005) applied ARIMA times series model to develop a forecasting model for global mean

temperature. In a similar vein, Kärner (2009) applied ARIMA time series to model long range temporal variability of total solar irradiance and surface air temperature time series.

Ford, Goranson et al (2005) used ARIMA time series model to estimate canopy transpiration based on sap flow obtained from *Pinus taeda* trees and multiple climatic variables that affect transpiration. The model explained 97% of the total variation in the data under both dry and wet conditions. The analysis revealed both an auto-regressive process (AR) and a moving average (MA) process.

3. Study area and data set

3.1. Description of the study area

The TP is situated in the western part of China between 80–105°E and 28–37°N. It is the highest plateau in the world and is characterized by mountain ranges with an average altitude of more than 4000 m above sea level, reaching the middle of the troposphere (Fu, Jiang et al. 2008). Figure 1 below shows different elevation classes over the Tibetan plateau.

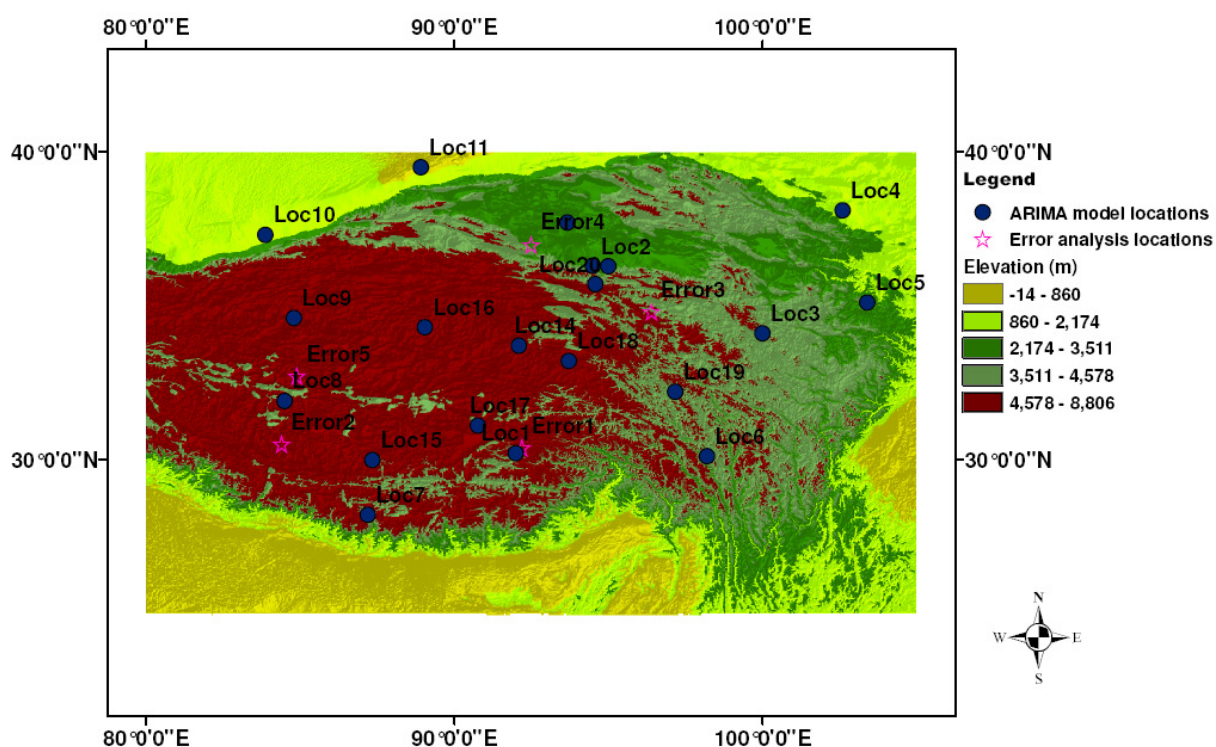


Figure 1: Digital elevation model of the Tibetan Plateau overlaid with locations of ARIMA model and Error analysis

The area is associated with mean annual total precipitation of 240 mm, with most of the precipitation occurring during the Asian summer monsoon system from May to September. Only a fraction of the total annual rainfall is brought by the winter monsoon. The mean monthly air temperatures are -10.3°C in January to 15.0°C in July. The summer monsoon is replaced by the winter monsoon by mid-October (Wen, Su et al. 2003; Zhang, Cheng et al. 2003; Herzsuh, Kramer et al. 2009).

3.2. SSM/I Data set

The SSM/I has been measuring brightness temperature since 1987. It is on board of the defence meteorological satellite program (DMSP), it has seven-channels, four-frequencies, and it is an orthogonally polarized passive microwave radiometer. (Wen, Jackson et al. 2005). Table 1 below shows the characteristics of SSM/I.

Table 1: Basic characteristics of SSM/I

Frequency (GHz)	Polarization H=horizontal V=vertical	Spatial resolution (km)	Passes A=Ascending D=descending
19.3	V & H	69x43	both
22.2	V	50x40	both
37.0	V & H	37x28	both
85.0	V& H	15x13	both

The brightness temperature data was downloaded from the National Snow and Ice Data Centre (NSIDC) (Maslanik and Stroeve 2009). LST and soil moisture were then retrieved from the brightness temperatures for further analysis using the specified algorithms in chapter 4. The LST was derived from the V- polarized 37GHz frequency while soil moisture was derived from the 19GHz frequencies of the SSM/I instrument.

3.3. Measured land surface data

LST and soil moisture measured at 4 cm soil depth were obtained from the archives of the faculty of geo-information Science and Earth observation (ITC), Tibetan plateau field station measurements. The measured data used in this study were of Naqu station (31.3°N, 91.9°E). The temperature data were for the years 2005 through 2008 while soil moisture data measured at 4 cm depth were for the years 2005 through June 2008. However, there were missing data especially for the first half of 2005 and the second half of 2007 in the case of measured LST.

4. LST and soil moisture retrieval methods

4.1. Passive Microwave theory

Passive microwave instruments measure surface emission in the range of 1 to 100 cm wavelength. Under vegetated conditions, part of the emitted radiation is from vegetation while another component is from the soil. The emitted radiation is related to land surface temperature and land surface emissivity through Rayleigh – Jeans approximation of Planck’s radiation function. Microwave radiation is almost exclusively dependent on emissivity in a given frequency, land surface temperature and atmospheric transmission which is close to 1 in the microwave domain (Dash, Gottsche *et al.* 2002).

$$T_B = \varepsilon T_S \quad [1]$$

Where T_B the microwave brightness temperature at a given frequency, ε is the smooth surface emissivity and T_S is the thermodynamic land surface temperature of the emitting land surface.

According to Kirchoff’s law of radiation, absorptivity is equal emissivity at a given wavelength (Dash, Gottsche *et al.* 2002) . It therefore follows that, since;

$$\alpha + R = 1 \quad [2]$$

$$R = 1 - \varepsilon \quad [3]$$

Where α is the absorptivity, R is the smooth surface reflectivity and ε is the land surface emissivity. The emitted land surface radiation is related to the relative permittivity (dielectric constant) of the soil through the Fresnel reflectivity function in the vertical and horizontal polarization (Ulaby, Moore *et al.* 1981)

$$R_V = \left[\frac{\varepsilon_r \cos \varphi - (\varepsilon_r - \sin^2 \varphi)^{0.5}}{\varepsilon_r \cos \varphi + (\varepsilon_r - \sin^2 \varphi)^{0.5}} \right]^2 \quad [4]$$

$$R_H = \left[\frac{\cos \varphi - (\varepsilon_r - \sin^2 \varphi)^{0.5}}{\cos \varphi + (\varepsilon_r - \sin^2 \varphi)^{0.5}} \right]^2 \quad [5]$$

Where R is the smooth surface reflectivity, V and H refers to vertical and horizontal polarizations, ε_r is the relative permittivity, φ is the satellite zenith angle (degrees).

4.2. Dielectric constant and soil moisture

Retrieval of soil moisture from passive microwave signals is based on the large differences in the dielectric constant of water ($\varepsilon_r=80$) and the dielectric constant of dry soil ($\varepsilon_r=3.5$) and the resulting dielectric properties of a soil-water mixture (Wang and Schmugge 1980; Dobson, Ulaby *et al.* 1985). Soil being a heterogeneous material i.e. composed, rocks/minerals, air and water, its dielectric properties is a function of soil moisture, soil salinity, soil texture and the frequency of the emitted radiation (Wang and Schmugge 1980; Dobson, Ulaby *et al.* 1985; Hallikainen, Ulaby *et al.* 1985).

4.3. Relationship between brightness temperature at 37GHz and LST

LST is the skin temperature of the Earth's surface and is a key component in various soil moisture retrieval algorithms (Magagi and Kerr 2001; Jackson, Hsu et al. 2002; Wen, Jackson et al. 2005; Sandells, Davenport et al. 2008; Liu, van Dijk et al. 2009). Previous studies have shown there is a linear relationship between the skin temperature and the brightness temperature at V- polarized 37 GHz channel (Owe, de Jeu et al. 2001; Holmes, de Jeu et al. 2009). In this study, measured LST was regressed on the brightness temperature for Naqu station for the period 2005 through July 2008 to derive land surface temperature for the simultaneous retrieval of soil moisture and vegetation transmissivity. Table 2 below summarizes the regression results, while figures 2 and 3 below demonstrate the goodness of fit of the model.

Table 2: Regression analysis of LST versus 37GHz v Pol. Brightness temperature

Coefficient	Estimate	Standard error	t-value	P-value	Statistical significance
Intercept	32.887	3.852	8.537	< 0.001	***
Slope	0.937	0.015	62.471	<0.001	***

Degree of freedom = 522, $R^2 = 0.882$, Residual standard error = 2.876k

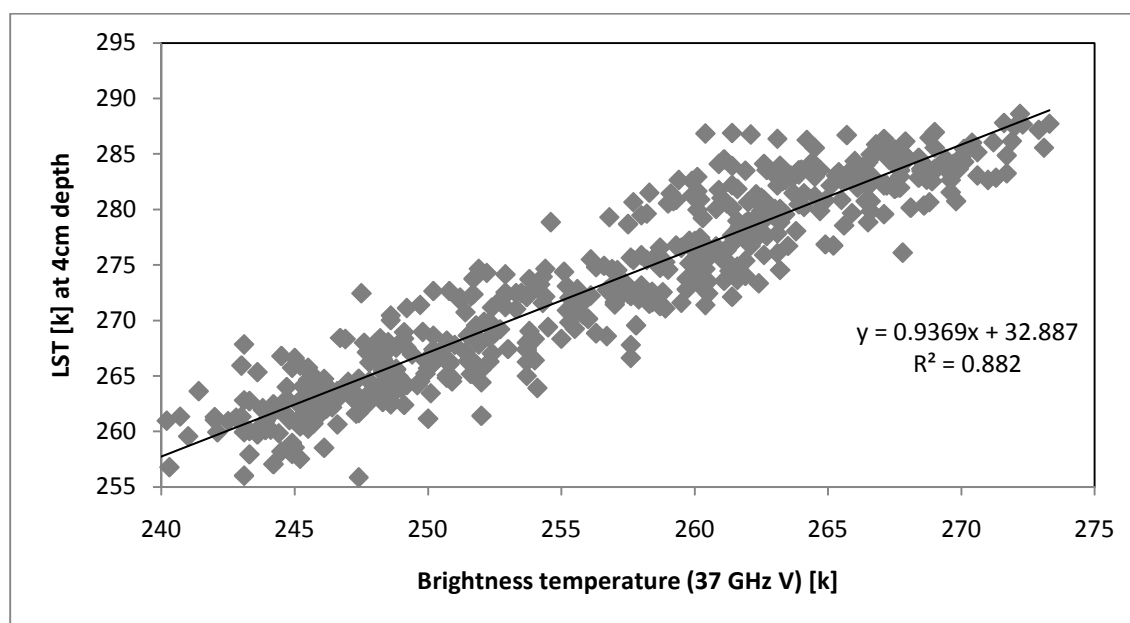


Figure 2: LST versus 37GHz vertical polarization brightness temperature

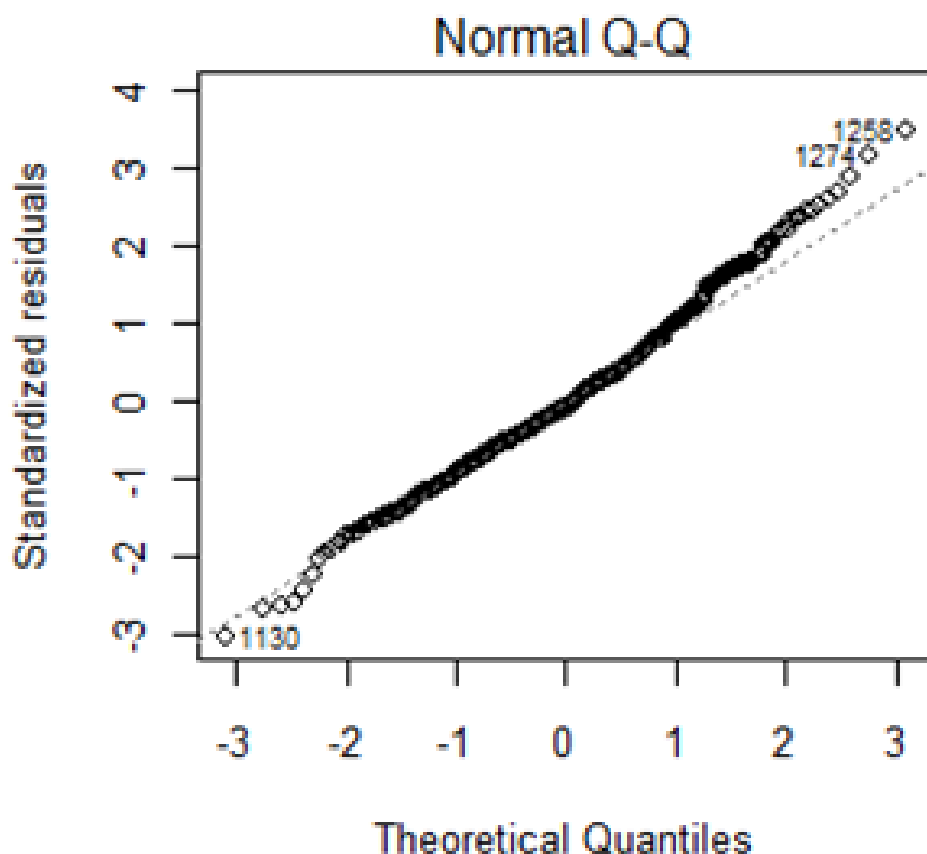


Figure 3: Normal probability plot of the residuals of LST vs 37GHz v.pol brightness temperature

Both the intercept and the slope are significantly different from zero at all levels of confidence and an examination of the normal Q-Q plot shows there is no need for data transformation. A high correlation coefficient and a relatively low residual standard error of 2.876K indicate the model has a good fit. The residuals are normally distributed with a mean of approximately zero. Therefore the land surface temperature over the TP was retrieved by using the relationship;

$$LST = T_{B37v}0.937 + 32.887 \quad [6]$$

4.4. Retrieval of land surface temperature, Soil moisture and vegetation transmissivity

4.4.1. Soil moisture retrieval algorithm

Soil moisture retrieval algorithms are generally based on the radiative transfer equation e.g. (Jackson 1997; Jackson, Hsu et al. 2002; Bindlish, Jackson et al. 2003; Wen, Jackson et al. 2005). Differences between methods are embedded in the procedure for correcting the influence of vegetation on soil moisture retrieval. In this study a similar algorithm was used based on the dual polarized channel 19.35 GHz of SSM/I to solve vertical and horizontal smooth polarized surface reflectivity. Through an iterative process, volumetric soil moisture, vegetation transmissivity and land surface temperature were retrieved by minimizing the difference between satellite measured brightness temperature at

19.35 GHz channel and simulated brightness temperature. An outline of the algorithm is shown in figure 4 below.

In this algorithm, two assumptions are made; the first assumption is that atmospheric effect on both 19GHz and 37GHz channels are negligible and the second assumption is that canopy temperature is equal to soil temperature. However, to ensure the second assumption holds true, the SSM/I data for the descending pass (morning hours) of F11, F13 and the ascending pass of F08 satellites were used in this study. This is because at this time of the day, thermodynamic temperature is relatively stable compared to during afternoon hours and therefore soil temperature can be assumed to be equal to canopy temperature (van de Griend and Owe 1994; Wen, Jackson et al. 2005)

4.4.2. Topp model

The commonly used dielectric mixing models for retrieving soil moisture are those of Dobson, Hallikainen and Wang-Schmugge (Wang and Schmugge 1980; Dobson, Ulaby et al. 1985; Hallikainen, Ulaby et al. 1985). However the drawback of these models is that they all require information on soil properties such as soil texture, soil porosity and wilting point which is not feasible to measure in an area the size of Tibetan plateau. On the other hand, the Topp model (G.C.Topp, J.L.Davis et al. 1980) does not require the input of soil texture, wilting point or vegetation water content. Moreover, de Jeu (2003) found that the influence of soil parameters on soil moisture retrieval were negligible. Consequently in this study the dielectric model of Topp was used. The model is given by;

$$\epsilon_r = 3.03 + 9.3\theta + 146\theta^2 - 79.7\theta^3 \quad [7]$$

Where ϵ_r is the dielectric constant and θ is the volumetric soil moisture

4.4.3. Vegetation effect on emissivity

The vegetation cover affects emissivity in two ways, not only does it emit its own radiation into the atmosphere but it also scatters and absorbs radiation emitted by the soil layer. Vegetation, therefore, acts as an attenuating and emissive layer above the soil, and the vegetation scattering is a function of vegetation water content, geometric structure, and spatial distributions of stem and leaf components (Njoku and Chan 2006). If the vegetation cover is too thick, most of the radiation measured by the satellite sensor will be emanating from the vegetation as soil emission is attenuated (Wigneron, Calvet et al. 2003). The radiative transfer equation of Mo, commonly referred to as the tau – omega model (Mo, Choudhury et al. 1982) accounts for the influence of vegetation on emissivity and therefore on the retrieved soil moisture. The model represents upwelling surface radiation in terms of brightness temperature and is given by;

$$T_B = (\epsilon\Gamma)T_s + (1 - \omega)(1 - \Gamma)T_c + (1 - \epsilon)(1 - \omega)(1 - \Gamma)IT_c \quad [8]$$

Where ϵ is the land surface emissivity, Γ is the vegetation canopy transmissivity, ω is the single scattering albedo and $T_c \approx T_s$ is the LST.

The first term of equation 8 accounts for the emission by the soil layer corrected for vegetation attenuation, the second term accounts for the emission by the vegetation only while the last term

accounts for the vegetation emitted radiation that interacts with the soil surface before being attenuated by the vegetation as it propagates into the atmosphere (Owe, de Jeu et al. 2001; Wigneron, Calvet et al. 2003).

The canopy transmissivity Γ determines how transparent the vegetation is to the microwave emission and is defined in terms of canopy optical thickness τ and the angle of incidence θ of the emitted radiation (Van de Griend and Owe 1993; van de Griend and Owe 1994; van de Griend, Owe et al. 1996; Bindlish, Jackson et al. 2003). Γ is defined as;

$$\Gamma = e\left(\frac{-\tau}{\cos\theta}\right) \quad [9]$$

4.4.4. Effect of surface roughness on emissivity

A rough surface has a larger surface area than a smooth surface, consequently surface roughness increases land surface emissivity and therefore increased brightness temperature measured by the satellite sensor at a given soil moisture condition (Wigneron, Calvet et al. 2003). The roughness parameter h is formulated as a function of the root mean square variation of surface height and the wave number which is a function of frequency (Choudhury, Schmugge et al. 1979; Wang and Choudhury 1981; Wang 1985; Njoku and Chan 2006). The empirical model of Wang and Choudhury (1981) was used in this study to correct land surface emissivity for surface roughness, because it accounts for depolarization caused by scattering of radiation between different surfaces.

Smooth Surface reflectivity is given by;

$$R = 1 - \varepsilon_{sur} \quad [10]$$

Where ε_{sur} is the surface emissivity

Surface reflectivity corrected for roughness is defined as;

$$R^p = [(1 - Q)R_o^p + QR_o^q]e^{(-k^2\delta^2\cos^2\varphi)} \quad [11]$$

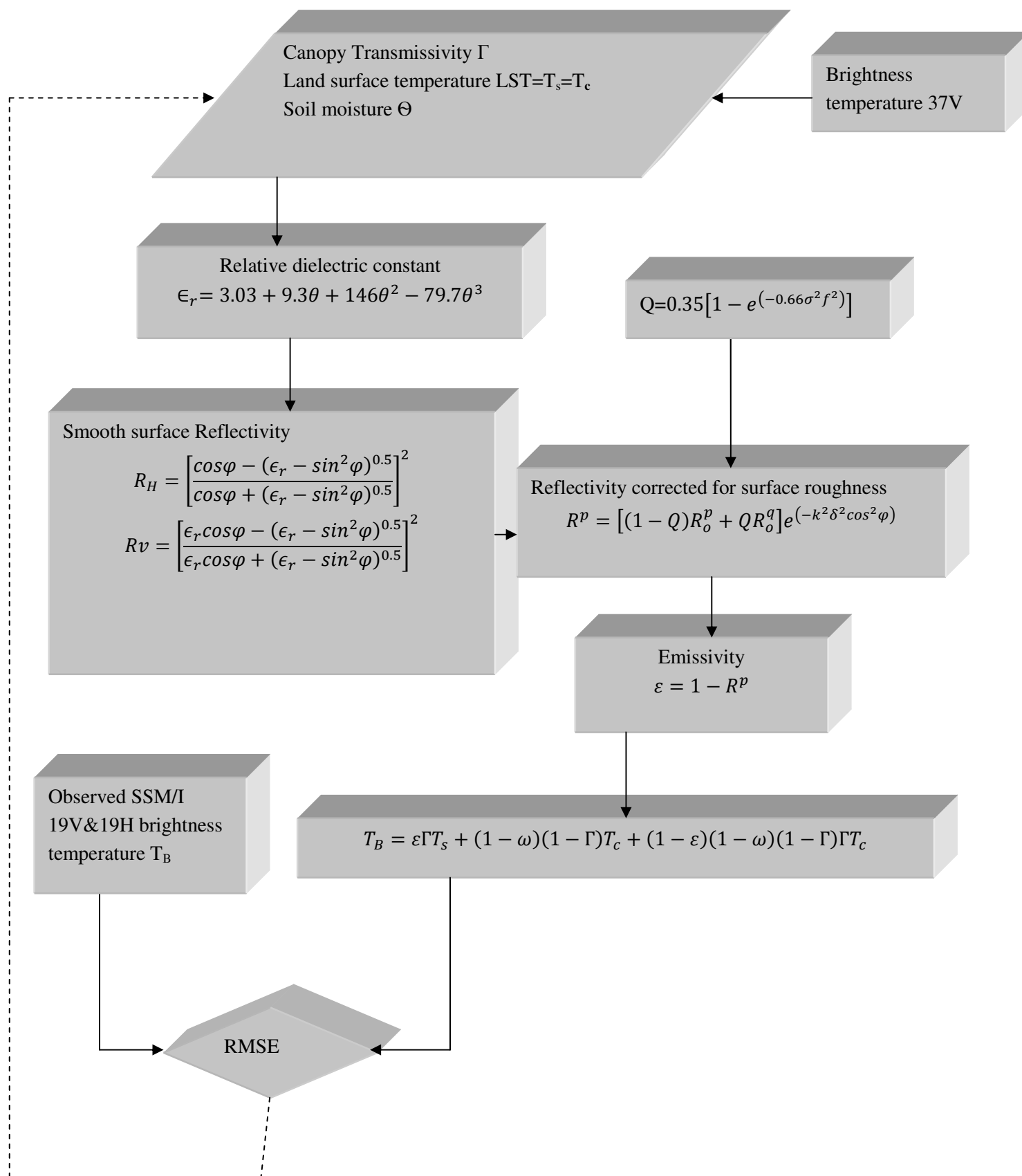
Where Q is a parameter that increases with surface roughness, R is the smooth surface reflectivity, p and q refer to orthogonal polarization, δ is the root mean square variation in surface height (cm), φ is the satellite viewing zenith angle (degrees) and k is the wave number given by $2\pi/\lambda$ (cm^{-1}). The parameter Q characterises both σ and the roughness correlation length. Kerr and Njoku (1990) estimated the parameter Q from equation 12 below.

$$Q = 0.35[1 - e^{(-0.66\delta^2f^2)}] \quad [12]$$

Where f is the frequency in GHZ

Figure 4 below is a schematic illustration of the soil moisture retrieval algorithm. Through the inversion of the tau - omega model, soil moisture and vegetation transmissivity are simultaneous retrieved. Initial soil moisture is used to compute the dielectric constant using Topp model. The resultant dielectric constant is then used to compute the smooth surface reflectivity in both the vertical and horizontal polarizations. The smooth surface reflectivity is then corrected for surface roughness using the method of Wang and Choudhury (1981). The reflectivity is then used to compute the

brightness temperatures. By minimizing the differences between the computed brightness temperatures and the brightness temperatures measured by the SSM/I sensor at 19GHz channel, the soil moisture and vegetation transmissivity are retrieved simultaneously.



Iteration till minimum root mean square error (RMSE) of T_B

Figure 4: Schematic diagram of LST, soil moisture and vegetation transmissivity retrieval

In literature surface roughness parameter h given by $\delta^2 k^2$, is thought to range between 0.0 and 0.4 (Owe, de Jeu et al. 2001). In this study, soil moisture over Naqu south station was compared to soil moisture retrieved using different values of surface roughness as shown in figure 5 below. A roughness parameter value of 0.0 cm yielded soil moisture in agreement with the ground measurements. The value of zero represents a flat surface which is characteristic of the TP and is consistent with finding from previous studies (Van de Griend and Owe 1993) , as a result a roughness parameter value of 0.0 cm was adopted for the study area.

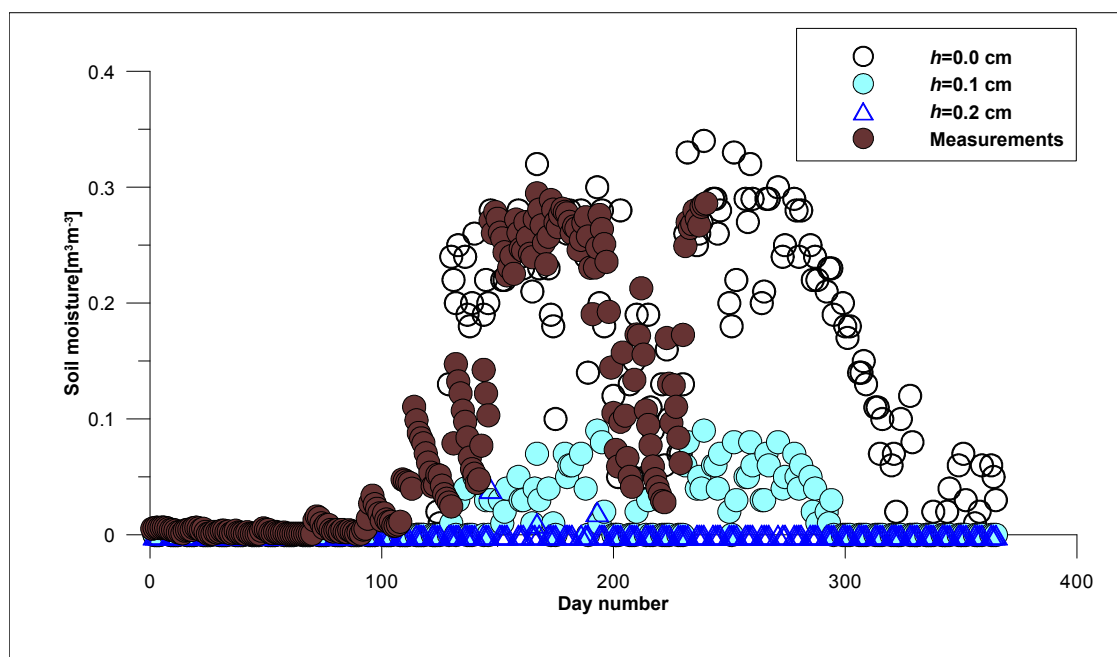


Figure 5: Influence of different values of surface roughness on retrieved soil moisture

4.4.5. Retrieval of soil moisture from frozen soils

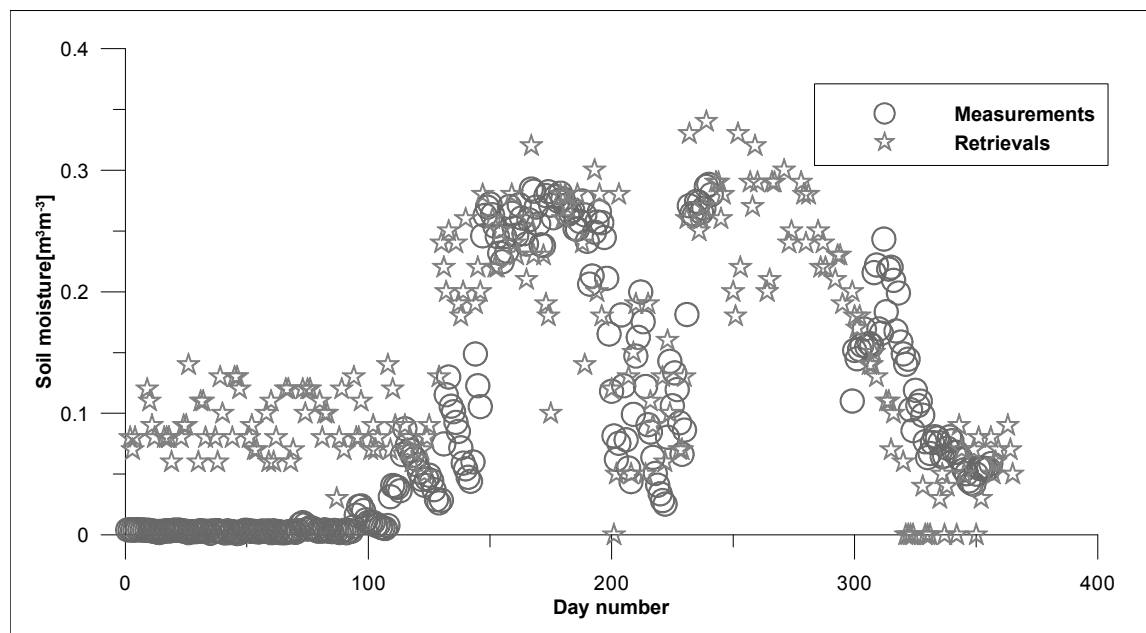


Figure 6: Effect of freezing on soil moisture retrieval (Naqu station 2006 data)

Wegmüller (1990) studied the effect of freezing and thawing on the microwave signatures of bare soils and concluded that frozen soils behave like dry soils because the liquid water content is small and in the range of 0 to $0.05 \text{ cm}^3 \text{ cm}^{-3}$. The LST model used to retrieve soil moisture in this study was derived from the relationship between surface temperature measured at 4cm soil depth and the brightness temperature at 37 GHz channel of SSM/I. During winter season, however, snow accumulates and soil freezes. Because frozen soils have higher emissivity than wet soils (Wegmüller 1990) due to the fact that water molecules in a frozen state are held tightly together to the extent that free rotation of water molecules is undermined and the surface temperature measured by the data logger is no longer at 4cm depth but rather 4cm plus snow depth, the soil moisture retrieved during the winter season is distorted as shown in the figure 6 above (day 0 -120).

This is largely due to increased emissivity caused by freezing and the increased depth of surface emission. To account for this effect, a surface roughness parameter of 0.05 was used for this period of the year. The results of the calibration is summarized in Fig. 7 below which compares measured soil moisture to soil moisture retrieved with two sets of roughness parameter h . i.e. 0.05 during freezing time of the year and 0.0 cm for the rest of the year. Panciera, Walker et al.(2009) proposed that, the dependence of surface roughness parameter on available soil moisture could be explained by the effect of volume scattering i.e. as available soil moisture diminishes, soil emission originates from deeper soil layers.

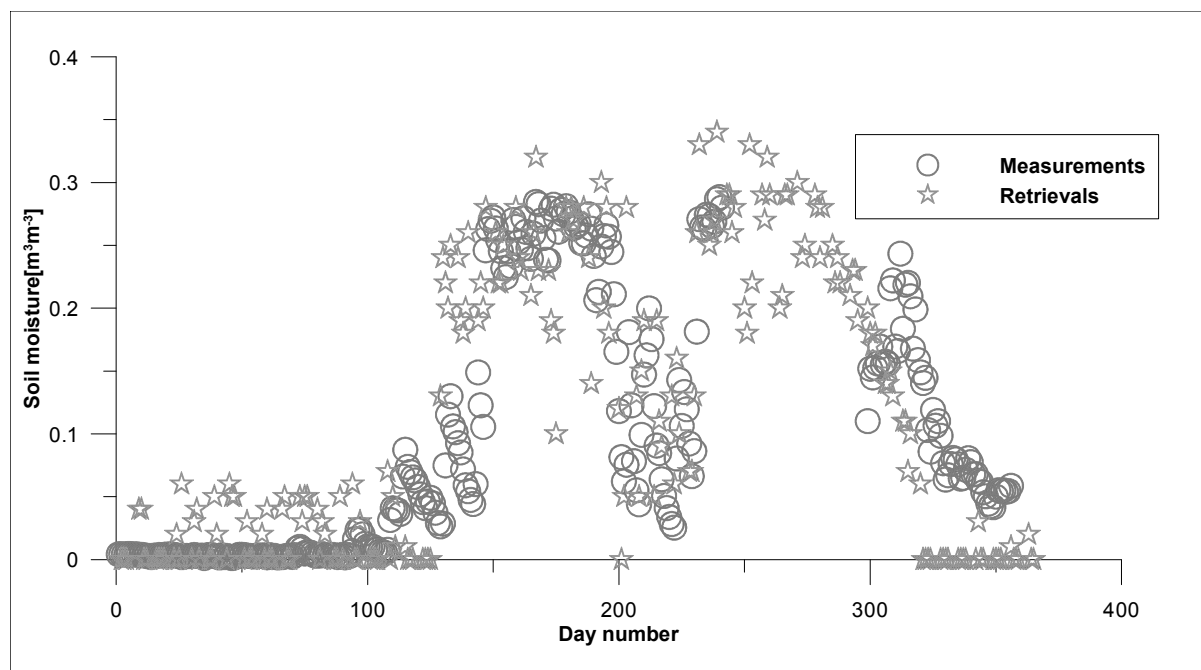


Figure 7: Calibration of soil moisture retrieval from a frozen soil (Naqu station 2006 data)

4.4.6. Effect of single scattering albedo on soil moisture retrieval

The single scattering albedo is a parameter which is a function of vegetation geometry and it directly affects the partitioning of the radiation emitted by the vegetation into scattering and absorption (Wen, Su et al. 2003). Several ranges of values are reported in literature e. g. van de Griend, Owe *et al.*(1996) reported a single scattering albedo of 0.06 to 0.12. similar values of single scattering albedo were presented by Lee and Anagnostou (2004). In this study the single scattering albedo was varied from 0.03 to 0.07 to investigate the suitable value for soil moisture retrieval over the Tibetan plateau. A single scattering albedo of 0.05, retrieved soil moisture which matched the measured soil moisture at Naqu site for the year 2006, consequently single scattering albedo of 0.05, was used for soil moisture retrieval over the Tibetan plateau. Figure 8 below summarizes the comparison between measured soil moisture and soil moisture retrieved with varying values of single scattering albedo

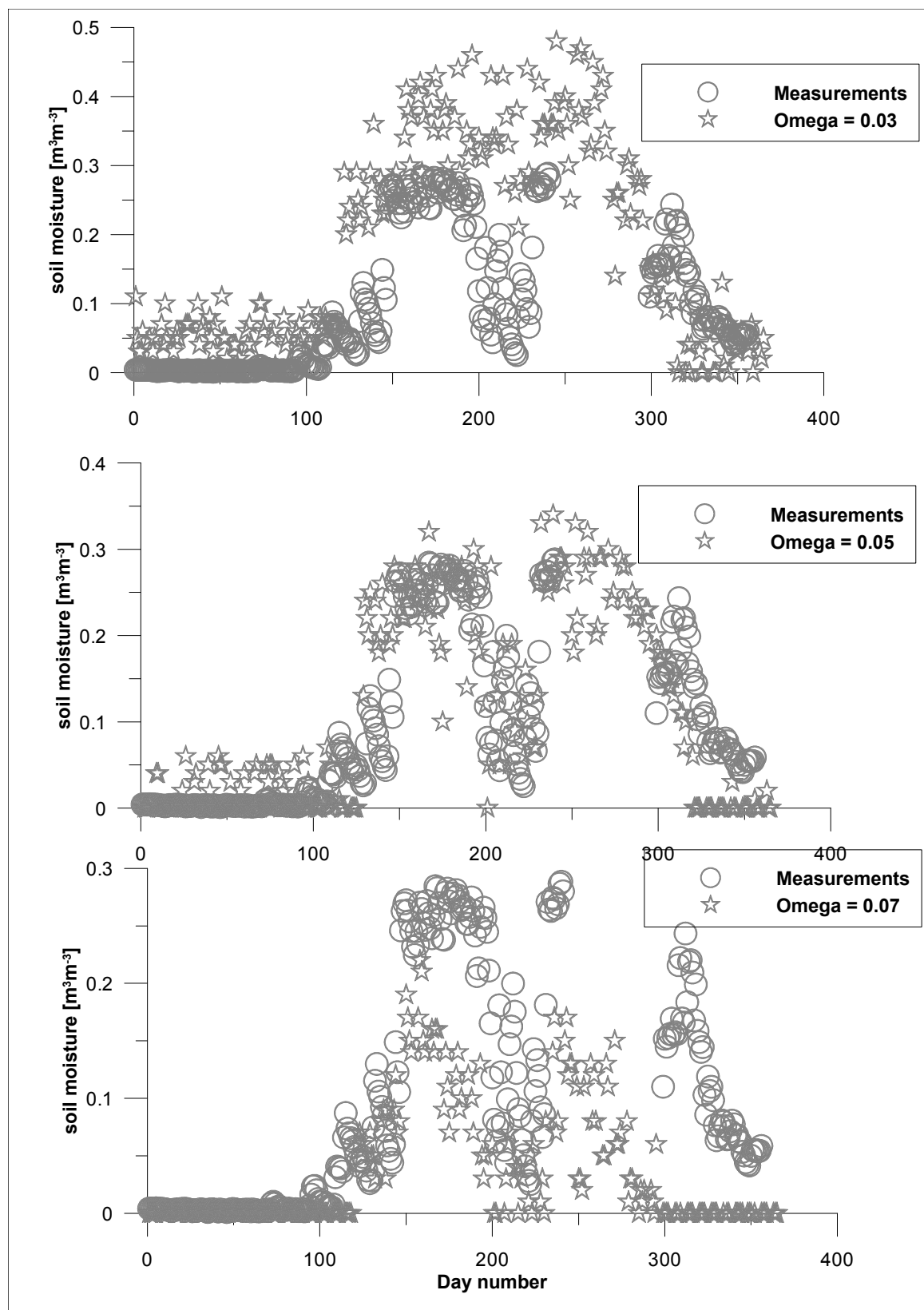


Figure 8: Effect of single scattering albedo on soil moisture retrieval (Naqu station 2006 data)

5. Results and discussions

The retrieved LST and soil moisture were compared to the ground measured LST and soil moisture for the periods 2005 through July 2008 as shown in figures 9 and 10 below. There is a good agreement between the retrieved land surface variable and ground measured variables

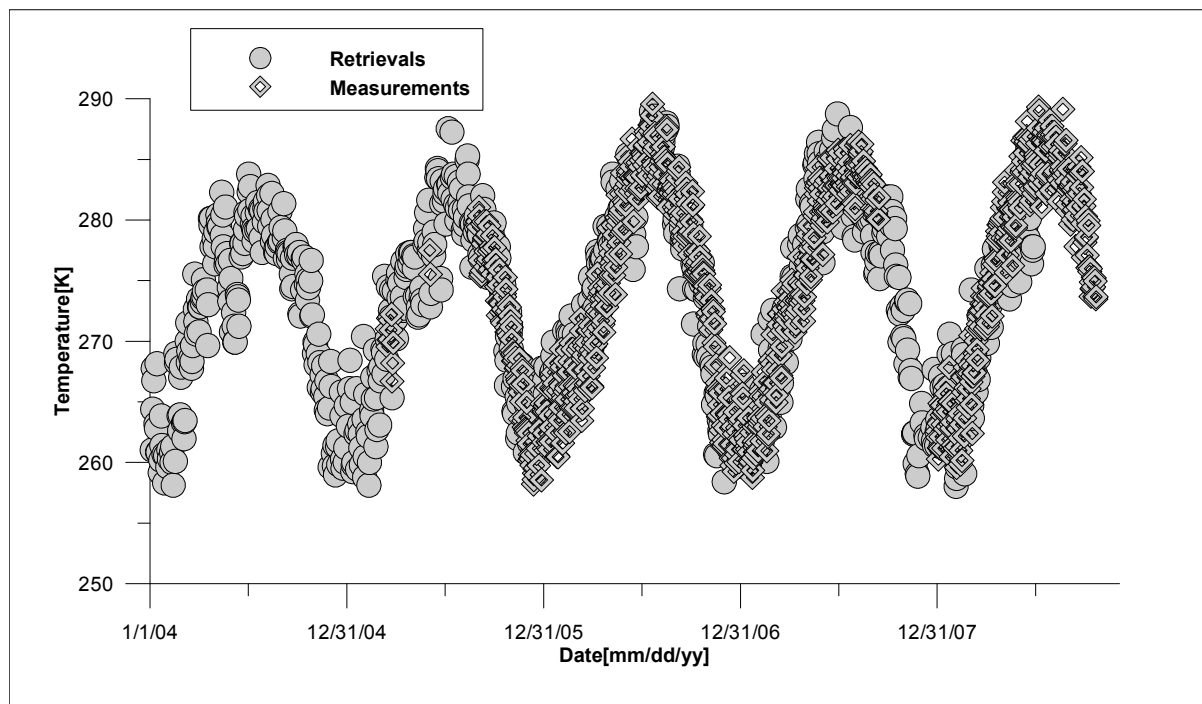


Figure 9: comparison between measured LST and retrieved LST

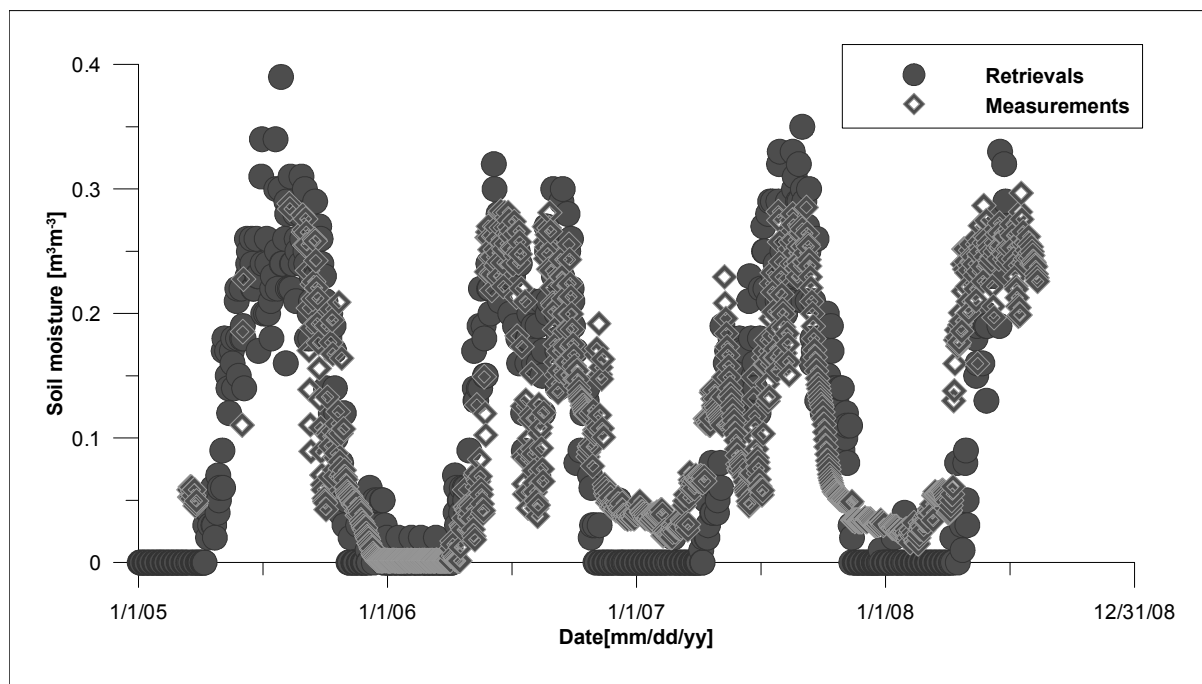


Figure 10: comparison between retrieved soil moisture and measured soil moisture

Single scattering albedo is generally thought to be time invariant (van de Griend and Owe 1994; Wen, Su et al. 2003), it was therefore justifiable to use a constant representative value of the single scattering albedo. The roughness parameter of 0.0 cm is a reasonable value for the Tibetan plateau and is in agreement with a value obtained for a similar environment (van de Griend and Owe 1994), considering the fact that the study area is a plateau interspaced with mountain ranges and is a semi arid area. However, the effect of volume scattering during the freezing conditions should be taken into account

The retrieved vegetation transmissivity showed seasonal variation with the highest value occurring during the peak of winter and the lowest value occurring during the peak of summer. This is expected because, during the peak of winter, vegetation on the Plateau becomes inactive and its biomass reduces, hence a higher transparency to microwave emission. On the other hand during the peak of summer nearly all the vegetation have full grown vegetation canopy, and therefore less transparent to the microwave emission. This is in agreement with the findings from previous studies of similar environment e.g. (Van de Griend and Owe 1993; van de Griend and Owe 1994). Figure 11 below shows the seasonal variation of vegetation transmissivity over the period from 2004 till 2008 on the Tibetan plateau.

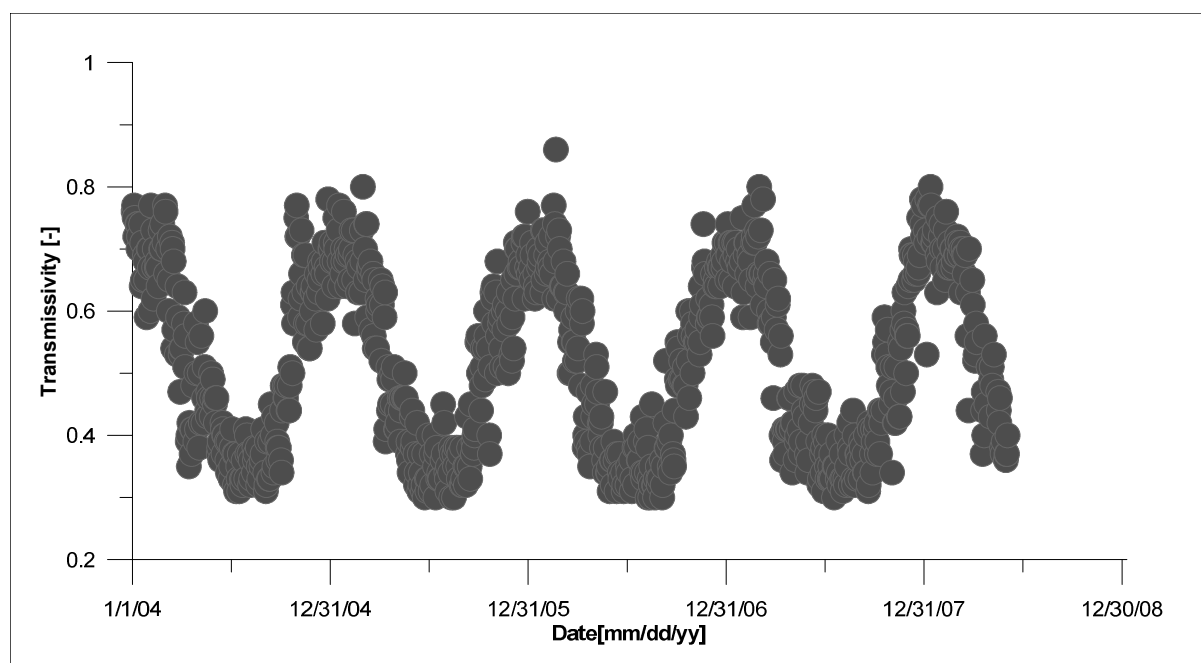


Figure 11: Retrieved vegetation transmissivity

The retrieval error for the land surface temperature was $0.00 \pm 2.87\text{k}$, this is quite in agreement with the algorithm of (Wen, Su et al. 2003) over central Tibetan plateau, while the soil moisture retrieval error was $0.00 \pm 0.04\text{m}^3\text{m}^{-3}$. Figure 12 below summarizes the error distribution of retrieved LST and soil moisture.

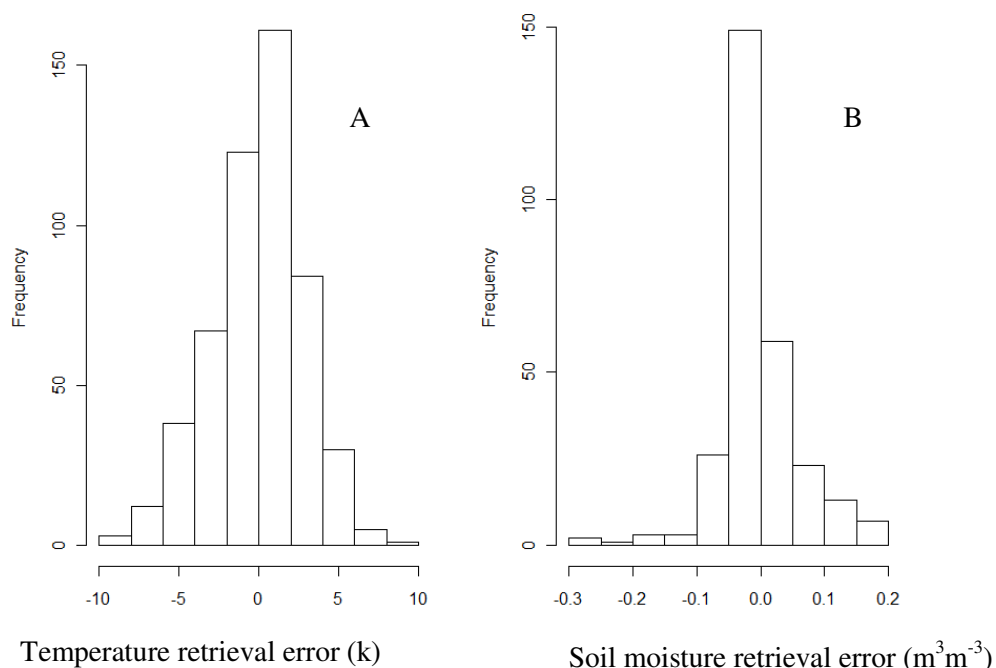


Figure 12: Histogram of LST retrieval error (A) and soil moisture retrieval error (B)

The temporal variation of soil moisture over the Tibetan plateau follows the monsoon sequence. From November to March the soil moisture is almost zero. However, as the monsoon season arrives in April (Zhang, Cheng et al. 2003) the moisture content begin to rise reaching its maximum value by July and dissipates by October. As shown in figure 13a soil moisture is highest in the south and eastern parts of the TP. This is partially attributed to the fact that the south eastern part of the TP is relatively low compared to the western section. See figure 1 above. Since fluids seek areas of least resistance to flow, the Indian monsoon winds are directed towards the south east. Hence, clouds release most of their water in that region of the TP. Areas with elevation of more than 4000m above sea level (western part) are significantly colder than regions with elevation below 4000m above sea level as shown in figure 13b. On the Plateau, specifically the large water bodies exhibit low temperatures. This is in agreement with the findings of Wen, Su et al. (2003). The low temperatures in the western part of the Tibetan plateau coupled with the influence of Taklamakan desert in the North West account for the low soil moisture in the western region of the TP.

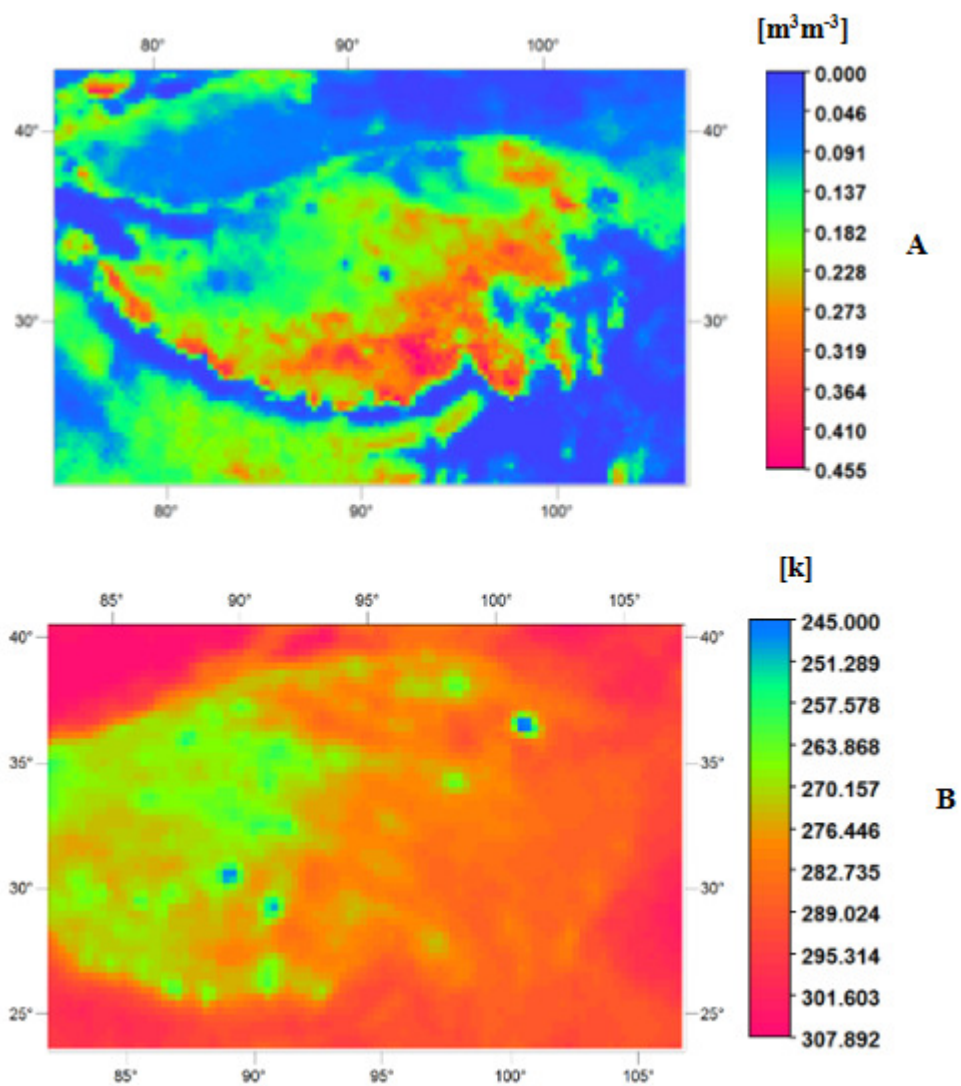


Figure 13: Spatial soil moisture (A) and LST (B) distribution over the Tibetan plateau (July 2004)

6. Evaluation of trend in the soil moisture and LST time series

Katz and Brown (1992), suggested that climate change is more evident as changes in variability rather than changes in averages. With a stack of 21 years of images, one of the retrievable measures of variability is the trend in soil moisture and temperature anomalies. A simple linear regression was fitted to the time series for every image pixel in the mean annual stack and the slope, standard error of the estimate and t-values of each trend line were assigned to corresponding pixels in the new soil moisture and temperature images (Liu and Chen 2000). Since monthly mean soil moisture and monthly mean temperature are autocorrelated, the trend analysis was done using soil moisture and temperature anomalies. The anomalies were computed by subtracting each, monthly mean soil moisture or temperature from the long term (21 year) monthly means (Hipel and Mcleod 1994).

Figure 14 below, show spatial patterns of simple linear trend in annual average soil moisture with the corresponding t -statistics. The critical t -value for a two tailed t-test is 2.09 at 5% level of significance. All t -values that fall outside of ± 2.09 are statistical significant at 95% confidence limits. Between 1987 and 2008, the western and northern part of the TP experienced an increasing significant soil moisture trend while the eastern and south eastern part of the TP showed no trend in soil moisture. This is in agreement with Zhao, Ping *et al.*(2004) who found that annual precipitation increased in the North western and the central part of the Tibetan plateau. The Taklamakan desert in the north western part of the TP experienced a decreasing significant soil moisture trend

Further examination of the spatial patterns of linear trend in monthly average normalized soil moisture anomalies indicate that, the increasing trends occurred during the summer monsoon seasons, i.e. April through October, while the decreasing trends occurred during the off summer monsoon season i.e. November through April. Wide spread positive trend in normalized soil moisture anomalies occurred during the months of April through July.

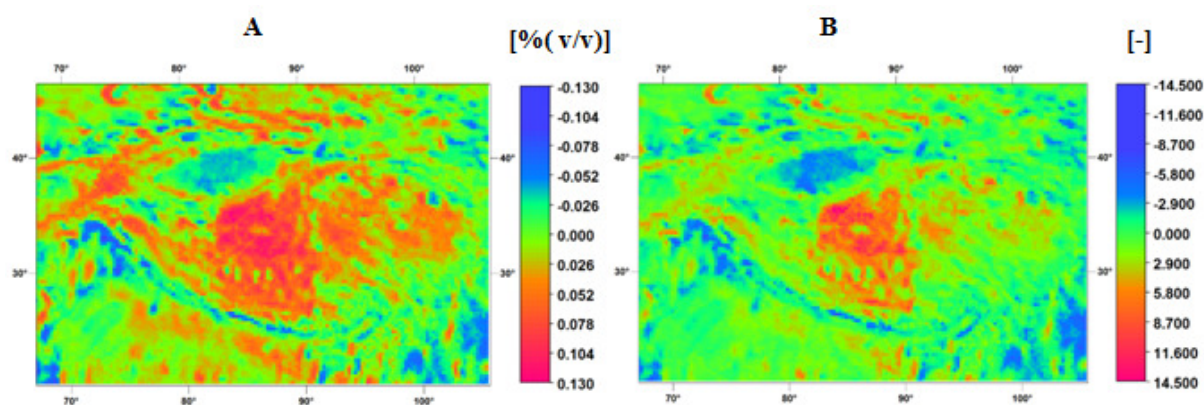


Figure 14: Trend in annual mean soil moisture anomalies (A) and corresponding t-Statistics (B)

While during the months of August through October, positive trend in normalized soil moisture anomalies were concentrated at the central part of the TP. This finding is in agreement with Liu, Wang *et al.*(2009) who demonstrated that two high elevation inland lakes at elevation of 4600m over

the central TP had increased in surface area by a maximum of 27.1% over an eight year period due to an increase in annual precipitation by 12.6% and increase in annual mean temperature by 0.41°C over the same period(1998-2005). A seasonal decomposition of the 21 year monthly soil moisture time series using loess procedure reveals a trend in soil moisture which is in agreement with the suggestion by Liu, Wang et al.(2009), that the changes in precipitation over the central TP was abrupt between 1996 and 2005 (figure 15 below).

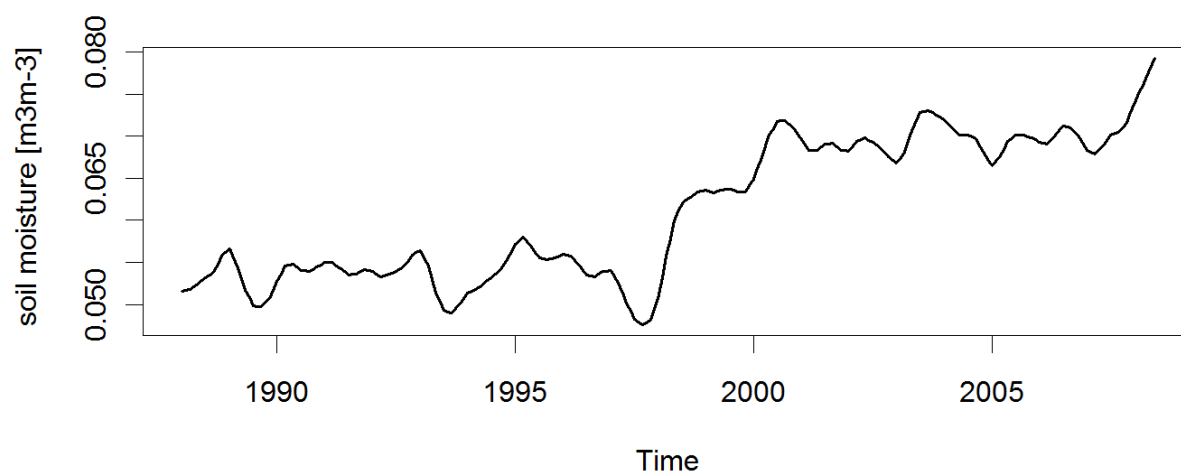


Figure 15: 21 year monthly mean soil moisture trend over the central TP

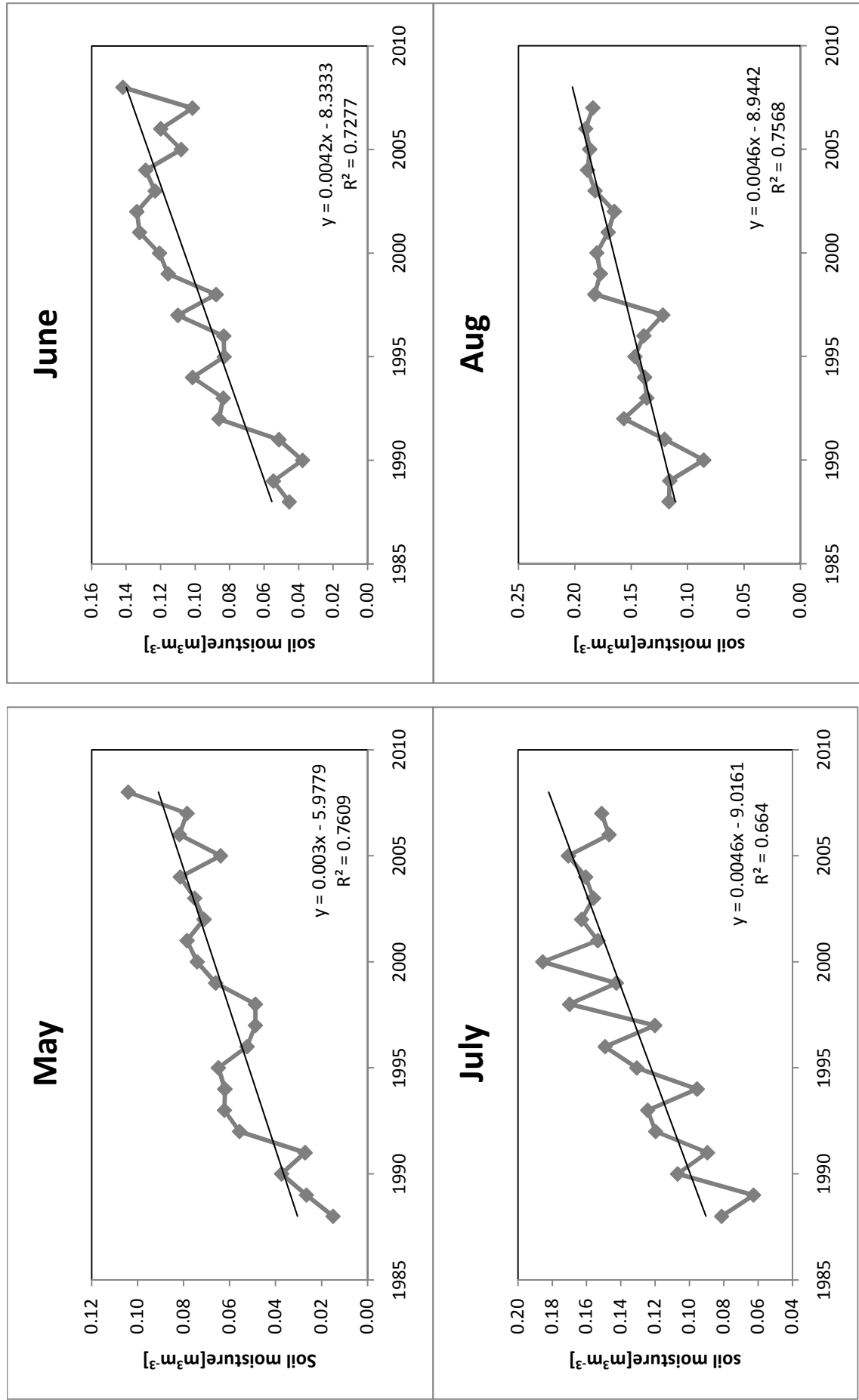


Figure 16: Trend in mean monthly soil moisture during the monsoon season

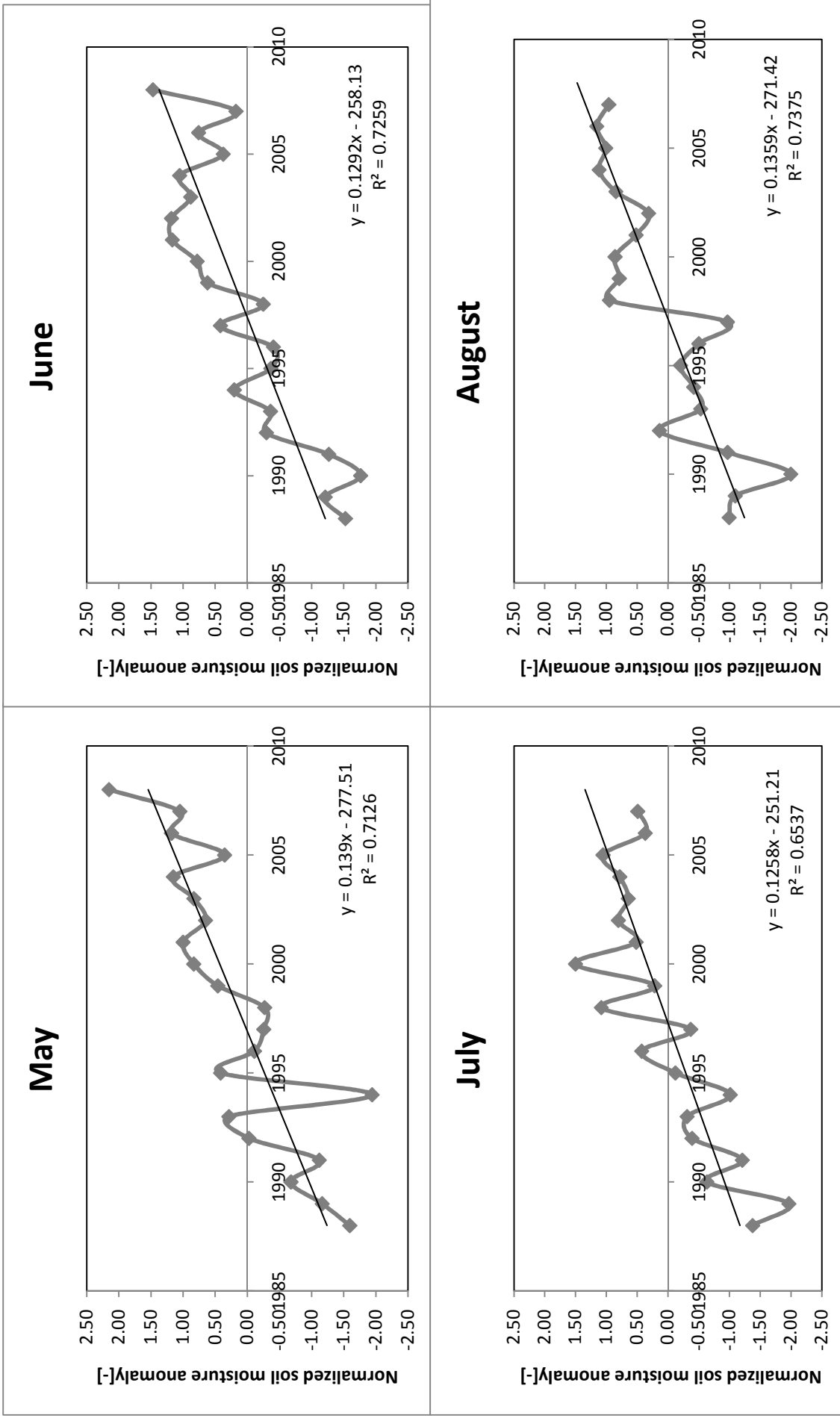


Figure 17: Normalized soil moisture anomaly magnitudes during the monsoon season

Figure 16 above shows that the average rate of soil moisture increment during the months of May through October (September and October are not shown) is $0.004\text{m}^3\text{m}^{-3}$ which is four times the annual rate. This is due to the fact that soil moisture contributed by the months of November through February to the total annual average is negligible. While figure 17 above demonstrates that the order of magnitude of the soil moisture anomalies is similar for all the 6 months and is in the range of ± 1.5 .

Figure 18 below demonstrates that between 1987 and 2008, the entire TP experienced significant warming. However, the central TP experienced more significant positive trend in land surface temperature anomalies. A similar trend is observed over scattered areas in the east and northern part of TP while the south and south eastern part of the TP experienced the least changes in temperature anomalies. This is in agreement with the findings of (Liu and Chen 2000; Liu, Cheng et al. 2009) who found that warming over the TP increases with increasing elevation. Zhao, Ping *et al.*(2004) found that the south eastern part of the TP had the least warming between 1967 and 2000. It should be noted that central and western TP has a significantly higher elevation than the south eastern part.

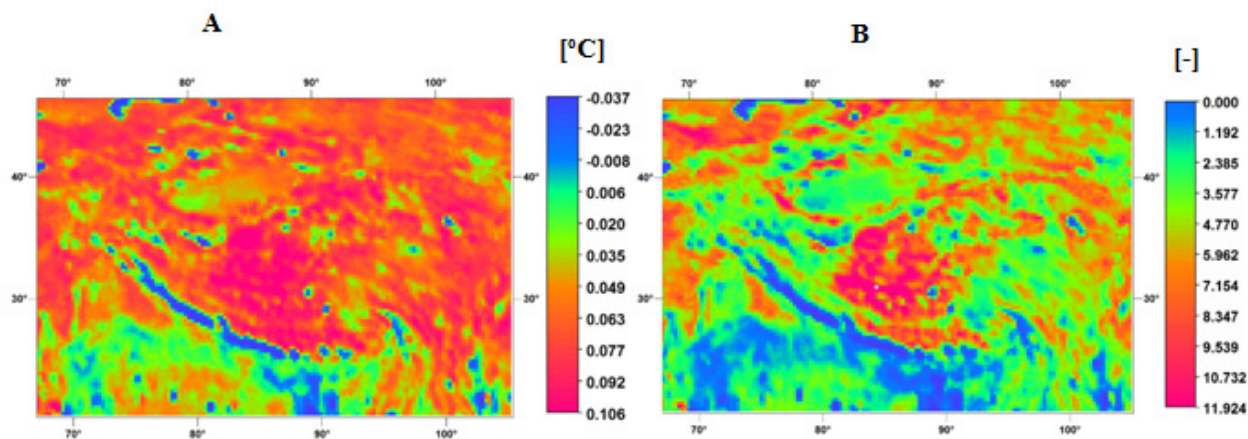


Figure 18: Trend in mean annual LST anomalies (A) and corresponding t-Statistics (B)

The overall warming trend over the TP of 0.1 to 1.1°C/decade is consistent with the finding of Trenberth, Jones et al. (2007). However, the central TP has warmed at the rate of 1.1°C /decade, which is 0.35°C above the global average of 0.75°C/decade (Trenberth, Jones et al. 2007). When viewed on monthly basis, the eastern part of the TP experienced more pronounced warming during the months of October through March. This is consistent with the findings of Liu and Chen (2000) and Liu, Cheng (2009) who found that warming in the eastern TP was more pronounced during the winter season. On the other hand the central and northern part of the TP experienced more pronounced warming during the months of May through October which is in agreement with the findings of Zhao, Ping et al.(2004)

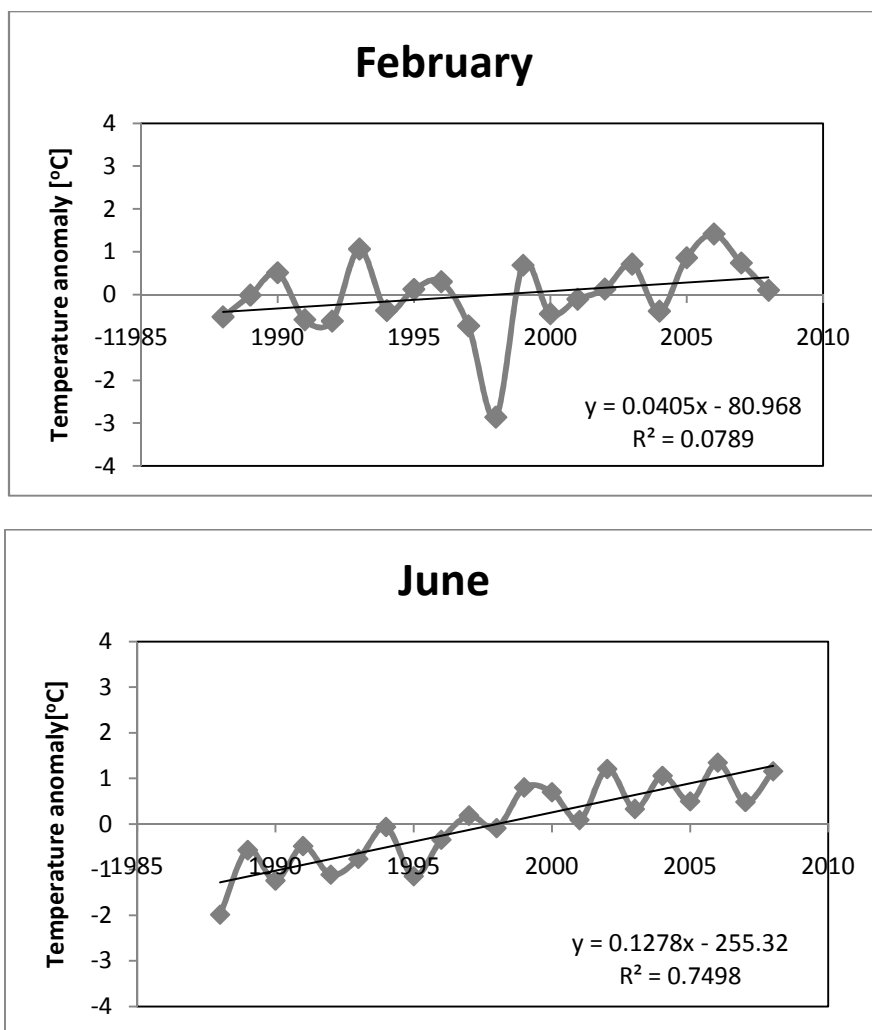


Figure 19: Comparison between warming during February and June

Figure 19 above shows that the annual rate of warming over the central TP was highest during the summer season at the rate of 1.3°C/decade while during the winter and spring season, the rate of warming was 0.41°C/decade. This is attributed to melting processing consuming much of the energy during the spring time and less energy spent on warming the surface.

7. Uncertainty and sensitivity analysis

7.1. Derivation of uncertainty matrix

The magnitude of errors caused by uncertainties in the input variables was computed using the error propagation analysis (deJeu 2003; Shi, Cheung et al. 2004; Puatanachokchai and Mikhail 2008). The brightness temperature errors were obtained from the SSM/I users guide (Hollinger, R. Lo et al. 1987). Although the variance of single scattering albedo and surface roughness are not known, the ranges of these parameters reported in literature were used to estimate their variances. The error propagation law is used to compute the standard deviation of the output variable by first generating the outputs using the reference variables and then changing the reference variables by 1% and generating the outputs once gain (Mikhail 1976). The difference between the outputs generated by the 1% change in input variable and the reference input variable is the error used to assess the reliability of the algorithm.

For simplicity the following symbols are used in the derivation of uncertainty matrix

Inputs (x)

Single scattering albedo	=	ω ,
Surface roughness	=	h ,
19GHz vertical	=	V ,
19GHz horizontal	=	H ,
37GHz vertical	=	k ,

Outputs (y)

Land surface temperature	=	T ,
Soil moisture	=	θ ,
Vegetation transmissivity	=	Γ .

The output y is a linear combination of input variables x and combination coefficient A_n where n represents the number of variables x . The combination coefficients are the partial derivatives of the outputs with respect to the inputs

$$y = \begin{bmatrix} T \\ \theta \\ \Gamma \end{bmatrix} \quad [13]$$

$$x = \begin{bmatrix} \omega \\ h \\ V \\ H \\ k \end{bmatrix} \quad [14]$$

The output y can be represented as a matrix denoted by;

$$y = A^T x \quad [15]$$

Where A^T is the transpose of matrix A

The covariance matrix of x is given by;

$$M(x) = \begin{bmatrix} \omega\omega & h\omega & \omega V & \omega H & \omega k \\ h\omega & hh & hV & hH & hk \\ V\omega & hV & VV & VH & Vk \\ H\omega & hH & HV & HH & Hk \\ k\omega & hk & kV & kH & kk \end{bmatrix} \quad [16]$$

It is assumed that there is no correlation between the variables x and therefore the covariance matrix of x reduces to;

$$M(x) = \begin{bmatrix} \sigma_{\omega}^2 & 0 & 0 & 0 & 0 \\ 0 & \sigma_h^2 & 0 & 0 & 0 \\ 0 & 0 & \sigma_v^2 & 0 & 0 \\ 0 & 0 & 0 & \sigma_H^2 & 0 \\ 0 & 0 & 0 & 0 & \sigma_k^2 \end{bmatrix} \quad [17]$$

The covariance matrix of y is given by;

$$M(y) = A^T M(x) A \quad [18]$$

And the matrix A is given by;

$$M(A) = \begin{bmatrix} \frac{\delta T}{\delta \omega} & \frac{\delta T}{\delta h} & \frac{\delta T}{\delta V} & \frac{\delta T}{\delta H} & \frac{\delta T}{\delta k} \\ \frac{\delta \theta}{\delta \omega} & \frac{\delta \theta}{\delta h} & \frac{\delta \theta}{\delta V} & \frac{\delta \theta}{\delta H} & \frac{\delta \theta}{\delta k} \\ \frac{\delta \Gamma}{\delta \omega} & \frac{\delta \Gamma}{\delta h} & \frac{\delta \Gamma}{\delta V} & \frac{\delta \Gamma}{\delta H} & \frac{\delta \Gamma}{\delta k} \end{bmatrix} \quad [19]$$

$$M(y) = \begin{bmatrix} TT & T\theta & T\Gamma \\ \theta T & \theta\theta & \theta\Gamma \\ \Gamma T & \Gamma\theta & \Gamma\Gamma \end{bmatrix} \quad [20]$$

Although there is no correlation between the input variables, the resultant variances, M(y) are correlated and is expanded to;

$$M(y) = \begin{bmatrix} \frac{\delta T}{\delta \omega} & \frac{\delta T}{\delta h} & \frac{\delta T}{\delta V} & \frac{\delta T}{\delta H} & \frac{\delta T}{\delta k} \\ \frac{\delta \theta}{\delta \omega} & \frac{\delta \theta}{\delta h} & \frac{\delta \theta}{\delta V} & \frac{\delta \theta}{\delta H} & \frac{\delta \theta}{\delta k} \\ \frac{\delta \Gamma}{\delta \omega} & \frac{\delta \Gamma}{\delta h} & \frac{\delta \Gamma}{\delta V} & \frac{\delta \Gamma}{\delta H} & \frac{\delta \Gamma}{\delta k} \end{bmatrix} \begin{bmatrix} \sigma_{\omega}^2 & 0 & 0 & 0 & 0 \\ 0 & \sigma_h^2 & 0 & 0 & 0 \\ 0 & 0 & \sigma_v^2 & 0 & 0 \\ 0 & 0 & 0 & \sigma_H^2 & 0 \\ 0 & 0 & 0 & 0 & \sigma_k^2 \end{bmatrix} \begin{bmatrix} \frac{\delta T}{\delta \omega} & \frac{\delta \theta}{\delta \omega} & \frac{\delta \Gamma}{\delta \omega} \\ \frac{\delta T}{\delta h} & \frac{\delta \theta}{\delta h} & \frac{\delta \Gamma}{\delta h} \\ \frac{\delta T}{\delta V} & \frac{\delta \theta}{\delta V} & \frac{\delta \Gamma}{\delta V} \\ \frac{\delta T}{\delta H} & \frac{\delta \theta}{\delta H} & \frac{\delta \Gamma}{\delta H} \\ \frac{\delta T}{\delta k} & \frac{\delta \theta}{\delta k} & \frac{\delta \Gamma}{\delta k} \end{bmatrix}$$

$$M(y) = \begin{bmatrix} \frac{\delta T}{\delta \omega} \sigma_{\omega}^2 & \frac{\delta T}{\delta h} \sigma_h^2 & \frac{\delta T}{\delta V} \sigma_v^2 & \frac{\delta T}{\delta H} \sigma_H^2 & \frac{\delta T}{\delta k} \sigma_k^2 \\ \frac{\delta \theta}{\delta \omega} \sigma_{\omega}^2 & \frac{\delta \theta}{\delta h} \sigma_h^2 & \frac{\delta \theta}{\delta V} \sigma_v^2 & \frac{\delta \theta}{\delta H} \sigma_H^2 & \frac{\delta \theta}{\delta k} \sigma_k^2 \\ \frac{\delta \Gamma}{\delta \omega} \sigma_{\omega}^2 & \frac{\delta \Gamma}{\delta h} \sigma_h^2 & \frac{\delta \Gamma}{\delta V} \sigma_v^2 & \frac{\delta \Gamma}{\delta H} \sigma_H^2 & \frac{\delta \Gamma}{\delta k} \sigma_k^2 \end{bmatrix} \begin{bmatrix} \frac{\delta T}{\delta \omega} & \frac{\delta \theta}{\delta \omega} & \frac{\delta \Gamma}{\delta \omega} \\ \frac{\delta T}{\delta h} & \frac{\delta \theta}{\delta h} & \frac{\delta \Gamma}{\delta h} \\ \frac{\delta T}{\delta V} & \frac{\delta \theta}{\delta V} & \frac{\delta \Gamma}{\delta V} \\ \frac{\delta T}{\delta H} & \frac{\delta \theta}{\delta H} & \frac{\delta \Gamma}{\delta H} \\ \frac{\delta T}{\delta k} & \frac{\delta \theta}{\delta k} & \frac{\delta \Gamma}{\delta k} \end{bmatrix}$$

$$\sigma^2 = \begin{bmatrix} \left(\frac{\delta T}{\delta \omega}\right)^2 \sigma_\omega^2 + \left(\frac{\delta T}{\delta h}\right)^2 \sigma_h^2 + \left(\frac{\delta T}{\delta V}\right)^2 \sigma_v^2 + \left(\frac{\delta T}{\delta H}\right)^2 \sigma_H^2 + \left(\frac{\delta T}{\delta k}\right)^2 \sigma_k^2 & \frac{\delta T}{\delta \omega} \frac{\delta \theta}{\delta \omega} \sigma_\omega^2 + \frac{\delta T}{\delta h} \frac{\delta \theta}{\delta h} \sigma_h^2 + \frac{\delta T}{\delta V} \frac{\delta \theta}{\delta V} \sigma_v^2 + \frac{\delta T}{\delta H} \frac{\delta \theta}{\delta H} \sigma_H^2 + \frac{\delta T}{\delta k} \frac{\delta \theta}{\delta k} \sigma_k^2 & \frac{\delta T}{\delta \omega} \frac{\delta \Gamma}{\delta \omega} \sigma_\omega^2 + \frac{\delta T}{\delta h} \frac{\delta \Gamma}{\delta h} \sigma_h^2 + \frac{\delta T}{\delta V} \frac{\delta \Gamma}{\delta V} \sigma_v^2 + \frac{\delta T}{\delta H} \frac{\delta \Gamma}{\delta H} \sigma_H^2 + \frac{\delta T}{\delta k} \frac{\delta \Gamma}{\delta k} \sigma_k^2 \\ \frac{\delta T}{\delta \omega} \frac{\delta \theta}{\delta \omega} \sigma_\omega^2 + \frac{\delta T}{\delta h} \frac{\delta \theta}{\delta h} \sigma_h^2 + \frac{\delta T}{\delta V} \frac{\delta \theta}{\delta V} \sigma_v^2 + \frac{\delta T}{\delta H} \frac{\delta \theta}{\delta H} \sigma_H^2 + \frac{\delta T}{\delta k} \frac{\delta \theta}{\delta k} \sigma_k^2 & \left(\frac{\delta \theta}{\delta \omega}\right)^2 \sigma_\omega^2 + \left(\frac{\delta \theta}{\delta h}\right)^2 \sigma_h^2 + \left(\frac{\delta \theta}{\delta V}\right)^2 \sigma_v^2 + \left(\frac{\delta \theta}{\delta H}\right)^2 \sigma_H^2 + \left(\frac{\delta \theta}{\delta k}\right)^2 \sigma_k^2 & \frac{\delta \theta}{\delta \omega} \frac{\delta \Gamma}{\delta \omega} \sigma_\omega^2 + \frac{\delta \theta}{\delta h} \frac{\delta \Gamma}{\delta h} \sigma_h^2 + \frac{\delta \theta}{\delta V} \frac{\delta \Gamma}{\delta V} \sigma_v^2 + \frac{\delta \theta}{\delta H} \frac{\delta \Gamma}{\delta H} \sigma_H^2 + \frac{\delta \theta}{\delta k} \frac{\delta \Gamma}{\delta k} \sigma_k^2 \\ \frac{\delta T}{\delta \omega} \frac{\delta \Gamma}{\delta \omega} \sigma_\omega^2 + \frac{\delta T}{\delta h} \frac{\delta \Gamma}{\delta h} \sigma_h^2 + \frac{\delta T}{\delta V} \frac{\delta \Gamma}{\delta V} \sigma_v^2 + \frac{\delta T}{\delta H} \frac{\delta \Gamma}{\delta H} \sigma_H^2 + \frac{\delta T}{\delta k} \frac{\delta \Gamma}{\delta k} \sigma_k^2 & \frac{\delta \theta}{\delta \omega} \frac{\delta \Gamma}{\delta \omega} \sigma_\omega^2 + \frac{\delta \theta}{\delta h} \frac{\delta \Gamma}{\delta h} \sigma_h^2 + \frac{\delta \theta}{\delta V} \frac{\delta \Gamma}{\delta V} \sigma_v^2 + \frac{\delta \theta}{\delta H} \frac{\delta \Gamma}{\delta H} \sigma_H^2 + \frac{\delta \theta}{\delta k} \frac{\delta \Gamma}{\delta k} \sigma_k^2 & \left(\frac{\delta \Gamma}{\delta \omega}\right)^2 \sigma_\omega^2 + \left(\frac{\delta \Gamma}{\delta h}\right)^2 \sigma_h^2 + \left(\frac{\delta \Gamma}{\delta V}\right)^2 \sigma_v^2 + \left(\frac{\delta \Gamma}{\delta H}\right)^2 \sigma_H^2 + \left(\frac{\delta \Gamma}{\delta k}\right)^2 \sigma_k^2 \end{bmatrix} \dots \dots \dots [21]$$

Note: equation 21 is a 3 x 3 matrix=equation 20. However, due to space limitations, it may not be clear to the reader. Column width ends at σ_k^2 . Equation 21 can be written as;

$$\sigma^2 = \sum_i^m \sum_j^n A_i A_j^T cov_{ij} \delta_{ij} \quad [22]$$

Where $\delta_{ij} = \begin{matrix} 0 : i \neq j \\ 1 : i = j \end{matrix}$ is the Kronecker delta function and A is the partial derivative of the output variables with respect to input variables

7.2. Results and discussions

Table 3: Magnitude of errors caused by a 1% uncertainty in the input variables of LST, soil moisture and vegetation transmissivity retrieval

variables	1% uncertainty level				
	Single scattering albedo	Surface roughness	Brightness temperature 19V	Brightness temperature 19H	Brightness temperature 37V
$\theta(\text{m}^3\text{m}^{-3})$	0.00196	0.00033	0.03708	0.00239	0.04440
T (k)	0.00000	0.00000	0.00000	0.00000	2.46221
$\Gamma[-]$	0.00072	0.00043	0.05234	0.05091	0.00885

Table 4: Relative contribution of input variables to the total standard deviation of LST, soil moisture and vegetation transmissivity

Lat	Lon	out put	STD	Single scattering albedo	Surface roughness	TB _{19V}	TB _{19H}	TB _{37V}
				% contribution of input parameters to total STD				
				$\sigma=0.085$	$\sigma=0.283$	$\sigma=0.8$	$\sigma=0.8$	$\sigma=0.6$
30.4°N	92.2°E	T	1.53	0	0	0	0	100
		θ	0.05	0	0	58.1	3.3	38.6
		Γ	0.06	0	0	43.6	56.0	0.4
30.5°N	84.4°E	T	1.48	0	0	0	0	100
		θ	0.04	0	0	55.2	0.3	44.5
		Γ	0.06	0	0	51.0	48.2	0.8
34.8°N	96.4°E	T	1.49	0	0	0	0	100
		θ	0.04	0	0	53.6	0.5	45.9
		Γ	0.06	0	0	50.2	47.2	2.6
37.0°N	92.5°E	T	1.52	0	0	0	0	100
		θ	0.02	0	0	57.8	0.1	42.1
		Γ	0.05	0	0	64.8	34.7	0.5
32.7°N	84.9°E	T	1.38	0	0	0	0	100
		θ	0.03	0	0	63.3	0	36.7
		Γ	0.05	0	0	60.8	37.7	1.5

Table 3 above summarizes the magnitude of retrieval errors caused by a 1% uncertainty in the input variables. An increase in the single scattering albedo, surface roughness and the brightness temperature at 19GHz V-polarization causes a decrease in the value of retrieved soil moisture while an increase in the brightness temperatures at 19GHz H-polarization and 37GHz V- polarization causes an increase in the retrieved soil moisture and the opposite holds true. On the other hand the reverse is true for the vegetation transmissivity.

The single scattering albedo and surface roughness contribution to the total standard deviation of the retrieved soil moisture is insignificant. See table 4 above. This finding is similar to the results of Wen, Su et al.(2003). de Jeu (2003) observed that single scattering albedo contributed only 2% and 1.5% to the total standard deviation of the retrieved soil moisture and vegetation optical depth respectively, in the Eurasian sites of his study. de Jeu (2003) also concluded that the influence of surface roughness to the retrieved soil moisture and vegetation optical thickness were negligible.

Error correlation is highest between LST- soil moisture and LST –vegetation transmissivity while the error correlation between soil moisture and vegetation transmissivity is relatively low i.e. 0.43, 0.50 and -0.1 respectively. The correlation is positive except for the soil moisture- vegetation transmissivity. All the correlations are significantly different from zero except for the soil moisture – vegetation transmissivity interaction. Therefore, statistically there is no correlation between the retrieval errors of soil moisture and vegetation transmissivity. However, a statistically significant correlation exists between the retrieval errors of land surface temperature and vegetation transmissivity and land surface temperature and soil moisture. This is largely due to the relatively large retrieval error of land surface temperature in comparison to the retrieval errors of soil moisture and vegetation transmissivity. See equation 21 above.

Soil moisture retrieval using the SSMI is sensitive to the 19GHz and 37GHz vertical polarizations while vegetation transmissivity is sensitive to the 19GHz vertical and horizontal polarization frequencies. Overall the retrieval errors of soil moisture and LST are comparable to other similar algorithms e.g. (Bindlish, Jackson et al. 2003; De Ridder 2003; Wen, Su et al. 2003; Wen, Jackson et al. 2005; Bindlish, Jackson et al. 2008; Draper, Walker et al. 2009)

8. Time series analysis (TSA)

8.1. Theory

Time series analysis is the procedure of fitting a stochastic process to a given time series and it entails three stages; model selection, model estimation and model verification. In this study, a family of TSA methods known as Auto Regressive Integrated Moving Average (ARIMA) (Piwowar and Ledrew 2002; Ford, Goranson et al. 2005) was used to analyze both the land surface temperature and soil moisture time series. A time-series model is characterized by three items; i.e. the orders, which are the numbers of lagged values that appear in the equation, the parameters, which are the associated coefficients and the actual values of the lags, if these differ from the progression $1...n$, where n is the number of lags (Castellano-Méndez, González-Manteiga et al. 2004).

An auto-regressive process (AR) is one which can be modelled as a function of the previous observations plus a random error. If Z_t variable measured at time t is a function β of the variable measured at an earlier time Z_{t-1} and the variable measured at a much earlier time p , Z_t is expressed as;

$$Z_t = \varepsilon_t + \sum_{i=1}^p \beta_i Z_{t-i} \quad [23]$$

Where t is the time of observation, $\beta_1, \beta_2, \dots, \beta_p$ are the AR parameters (coefficients), ε is the random error at time t , p is the order of AR and the model is written as AR(p).

A moving average process (MA) on the other hand, is one which can be modelled as a function of the random error of the previous observation. Considering the above example and replacing p with q , the variable Z_t is expressed as ;

$$Z_t = \mu + \sum_{i=1}^q \gamma_i \varepsilon_{t-i} \quad [24]$$

Where $\gamma_1, \gamma_2, \dots, \gamma_q$ are the MA parameters (coefficients), ε is the random error at a given time, q is the order of the MA and the model is written as MA(q). For a stationary ARIMA model consisting of a non seasonal and seasonal component of the form ARIMA (pdq)(PDQ) m , the model is expressed as;

$$Z_t = \sum_{i=1}^p p_i Z_{t-1} + \sum_{i=1}^q q_i \varepsilon_{t-1} + \sum_{i=1}^P P_i Z_{t-im} + \sum_{i=1}^Q Q_i \varepsilon_{t-im} + \varepsilon_t \quad [25]$$

Where p is the order of AR, d , is the frequency of non seasonal differencing, q is the order of MA, and P, D, Q and m represent the seasonal order of AR, seasonal frequency of differencing, seasonal order of MA and m is the period of the series which for most seasonal data equal to 12 (Castellano-Méndez, González-Manteiga et al. 2004). For differenced time series, Z_t is replaced with the differenced values ΔZ_t . The steps for the application of an ARIMA model to the time series of SSM/I retrieved soil moisture and land surface are shown in figure 20 and described below.

8.2. Model selection

Soil moisture and LST time series plots for randomly selected 20 pixels were visually inspected and analyzed for properties such as trends, periodicity, changes in the variance, changes in the mean and

presence of outliers in the series. The objectives of this step are three folds:(i) to identify the presence or absence of trends in the environmental variables over time; (ii) to evaluate the need for data transformation required to model the correlation structure in the time series; (iii) to determine the orders of AR and MA in a given time series (Piwowar and Ledrew 2002; Yurekli and Kurunc 2006). Both the plots of soil moisture and LST series have strong seasonal characteristics, with the highest values recorded in summer and the lowest values recorded in winter.

The data was further decomposed into its seasonal component, trend and residuals (figure 21 below). The seasonal and trend decomposition procedure using “loess” (STL), which is a non parametric regression technique was used to decompose the given series by determining the trend using “LOcally wEighted regreSsion Smoother (Loess)” technique, followed by deduction of the trend from the series to obtain the seasonal component and the residuals (Li, Campbell et al. 2003; Zuur and Pierce 2004; Verbesselt, Hyndman et al. 2009). The seasonal decomposition confirmed the presence of a positive trend in both the soil moisture and LST time series. The general “loess” model is given by;

$$Z_t = T_t + S_t + \varepsilon_t \quad [26]$$

Where Z_t is the univariate time series, T_t is the trend, S_t is the seasonal component and ε_t is the random error

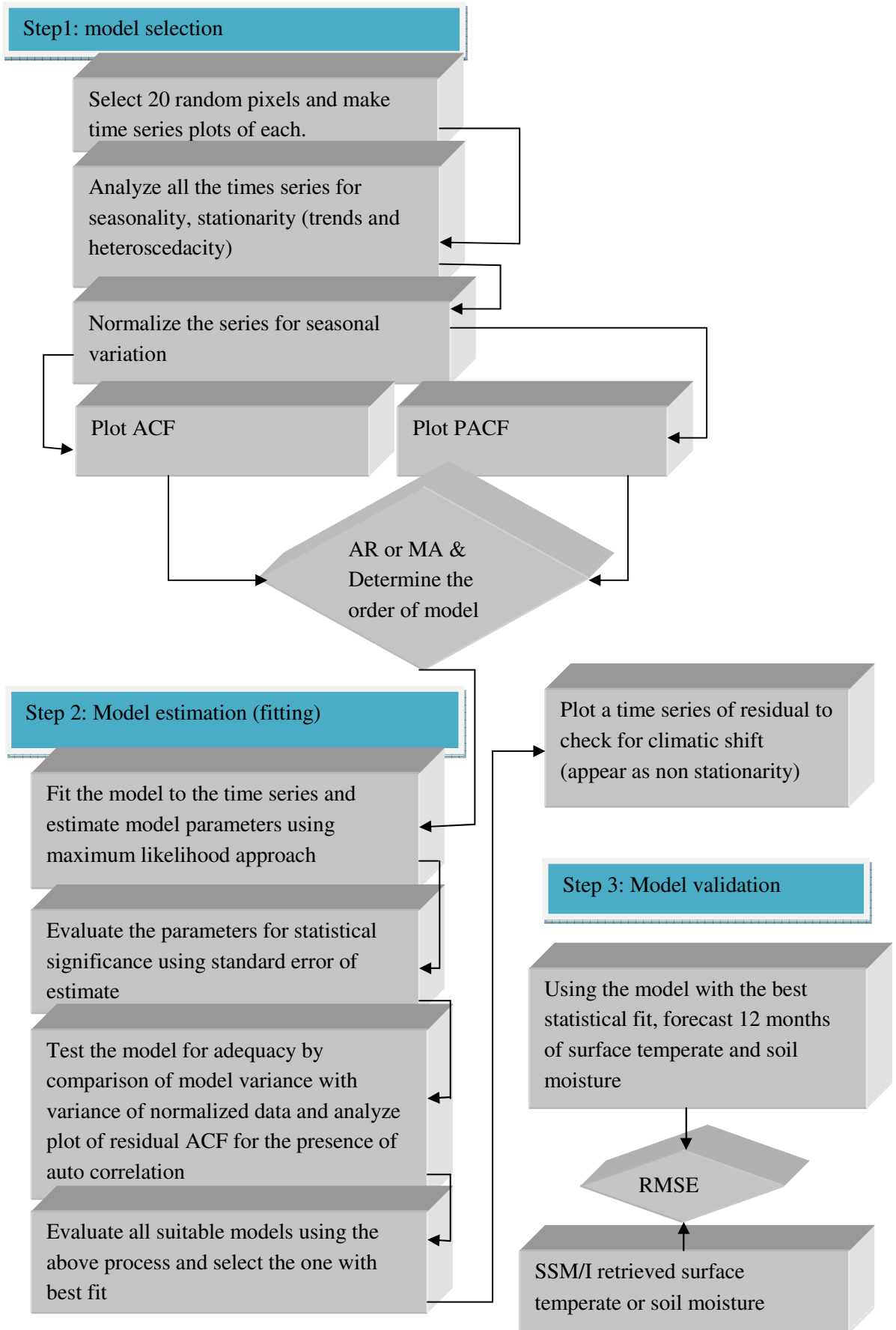


Figure 20: Schematic illustration of ARIMA modelling of soil moisture and LST

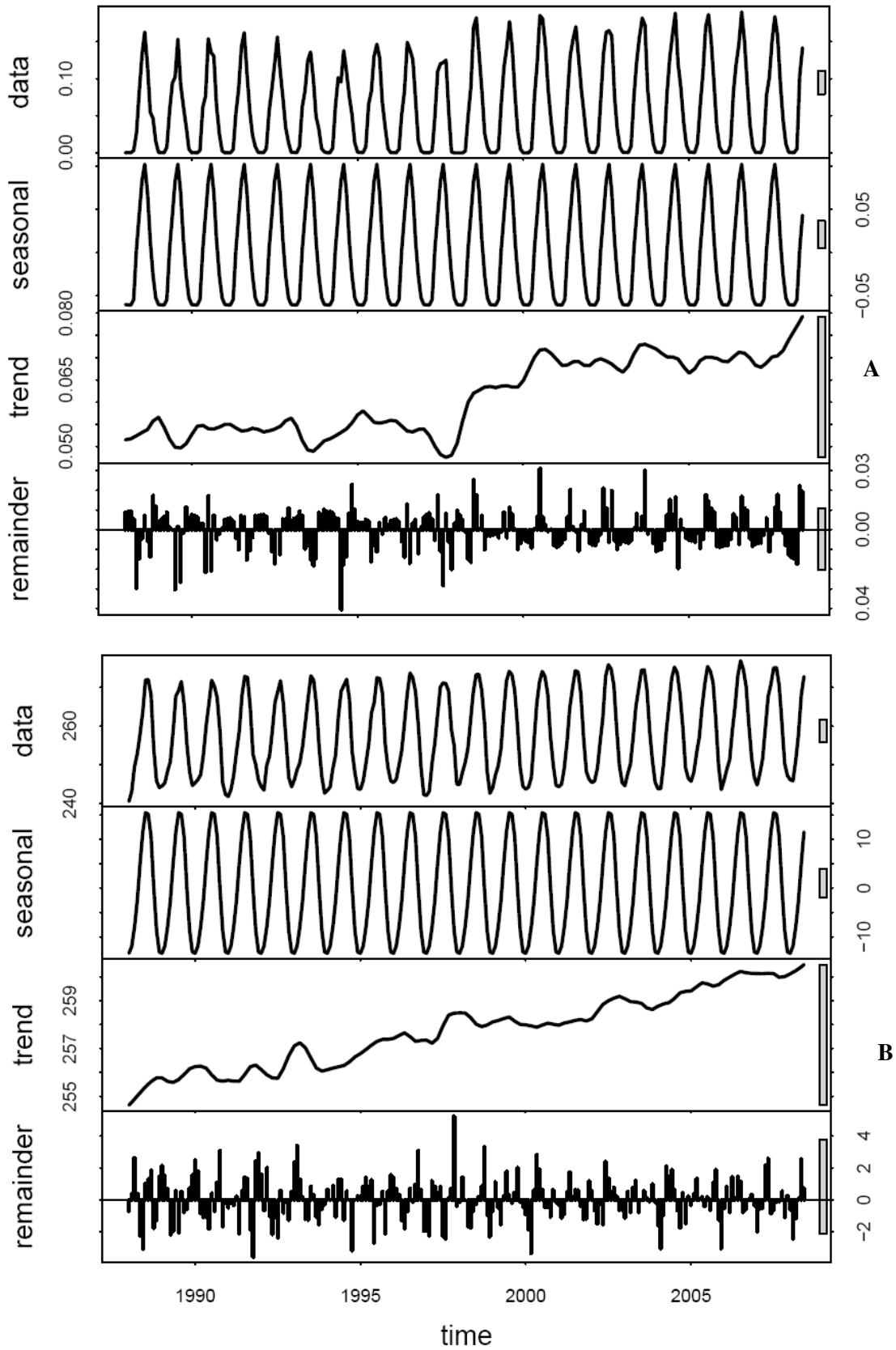


Figure 21: Decomposed soil moisture (m³m⁻³) [A] and LST(k) [B]

Modelling the correlation structure in a time series is done on a stationary time series, i.e. one with a constant mean and constant variance. In a stationary time series, the covariance between two observations Z_t and Z_{t+k} is a function of the lag k (difference between observation times) of the two observations and is independent of the time t in the series.

Evaluation of a suitable ARIMA model was done through the comparison of sample autocorrelation functions (ACF) and the sample partial autocorrelation functions (PACF) of the soil moisture and LST residuals with the theoretical values (Cimino, Del Duce et al. 1999; Piwowar and Ledrew 2002; Kärner 2009). The ACF is the measure of linear dependence between observations. While the PACF is the measure of the correlation remaining after the auto correlation in time series has been accounted for.

For a given observation Z_t , the expectation of Z_t is given by;

$$E(Z_t) = \mu_t \quad [27]$$

And its variance is given by;

$$\sigma_t^2 = E(Z_t - \mu_t)^2 \quad [28]$$

The auto correlation function can be derived by normalizing auto covariance (dividing by standard deviation) of Z_t which is given by;

$$\gamma(t_1 t_2) = E[(Z_{t_1} - \mu_{t_1})(Z_{t_2} - \mu_{t_2})] \quad [29]$$

$$r(t_1 t_2) = \frac{E[(Z_{t_1} - \mu_{t_1})(Z_{t_2} - \mu_{t_2})]}{\sigma_{t_1} \sigma_{t_2}} \quad [30]$$

Where γ is the covariance of Z , r is the auto correlation of Z , μ is the mean of Z , σ_{t_1} and σ_{t_2} are the standard deviation of Z at time t_1 and t_2 respectively.

For observations, Z_1, Z_2, \dots, Z_n , the observations are paired and treated as a bivariate data to estimate the auto correlation between consecutive pairs $(Z_1, Z_2), (Z_2, Z_3), \dots, (Z_{n-1}, Z_n)$ at a given lag k defined by;

$$r_k = \frac{\sum_{i=1}^{n-k} (Z_i - \mu_z)(Z_{i+k} - \mu_z) / (n-k)}{\sum_{i=1}^n (Z_i - \mu)^2 / n} \quad [31]$$

Where n is the length of the time series and k is a given lag (Slini, Karatzas et al. 2002)

Similar to correlation, the auto correlation ranges between -1 and 1 and in the determination of model orders, the ACF and PACF serve to complement each other since they display contrasting characteristics. The ACF plot attenuate for an AR process, while it truncates for a MA process and is not significantly different from zero after lag q , meanwhile the PACF plots truncate for an AR process and is not significantly different from zero after lag p and it attenuates for a MA process (Piwowar and Ledrew 2002; Yurekli and Kurunc 2006; Yürekli, Simsek et al. 2007). The characteristic plots are shown in (figures 26 and 27 below). For twenty lags an auto correlation coefficient may fall outside the 95% confidence limit only once by chance.

The ACF is not a valuable time series analysis tool for non stationary time series data. Consequently, seasonal variation and trends in land surface temperature and soil moisture were normalized before

analysis. Achieving stationarity of the time series required two stage approaches, for both land surface temperature and soil moisture to eliminate both the trend and periodicity.

The common methods for de-seasonalizing time series are, seasonal differencing, subtracting monthly averages from the time series (anomalies), periodic function modelling, and the derivation of indicator variables for individual months (Brockwell and Davis 1996; Chatfield 2003). Each of these methods have drawbacks (Zuur and Pierce 2004). However, comparison of methods is outside the scope of this research and therefore a periodic function which has only three parameters as opposed to indicator variables which has twelve parameters was opted for, for this research. A periodic function was first fitted to the data and the resultant residuals were differenced once to obtain stationary soil moisture and temperature residuals for the complete time series analysis (Brockwell and Davis 1996; Castellano-Méndez, González-Manteiga et al. 2004). Tables 5 and 6 below summarize the periodic functions of LST and soil moisture respectively. Figures 22 and 23 below are the plots of LST and soil moisture residuals of periodic functions respectively

The periodic function is given by;

$$Z_t = \beta_0 + \beta_1 \sin\left(\frac{2\pi}{12}t\right) + \beta_2 \cos\left(\frac{2\pi}{12}t\right) + \varepsilon_t \quad [32]$$

Where Z_t is the time series variable, β_0 is the intercept, β_1 and β_2 are the coefficients of the sine and cosine functions respectively and ε_t is the random error component of the periodic function.

Table 5: Summary of LST periodic function at location 12

coefficient	Estimate	Std error	t-value	P-value	Statistical significance
β_0	257.746	0.1596	1615.05	< 0.001	***
β_1	-8.6144	0.2257	-38.17	< 0.001	***
β_2	-12.2319	0.2256	-54.21	< 0.001	***

df=243, $R^2=0.94$, residual std error=2.968

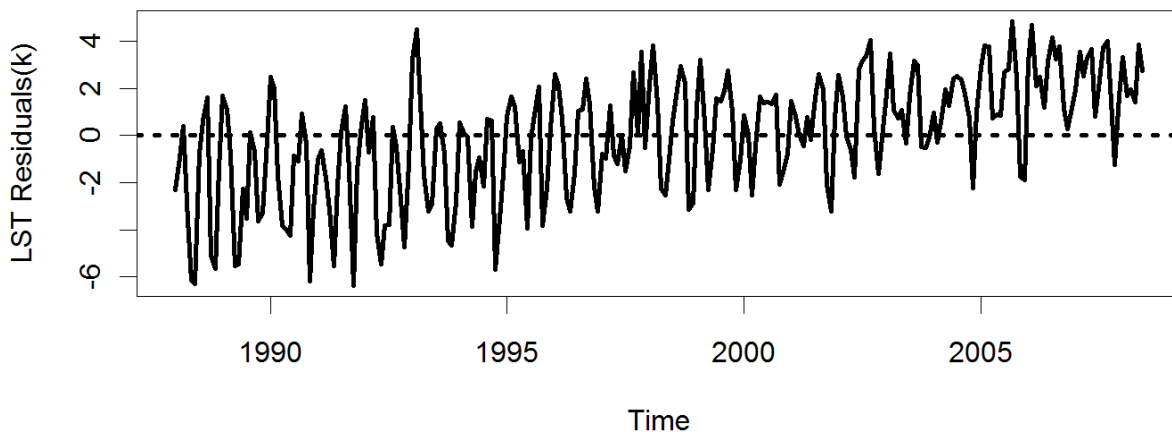


Figure 22: Land surface temperature residuals after eliminating periodicity (location 12)

Table 6: Summary of soil moisture periodic function at location 16

coefficient	Estimate	Std error	t-value	P-value	Statistical significance
β_0	0.0610	0.0013	48.29	< 0.001	***
β_1	-0.0642	0.0018	-35.91	< 0.001	***
β_2	-0.0487	0.0018	-27.23	< 0.001	***

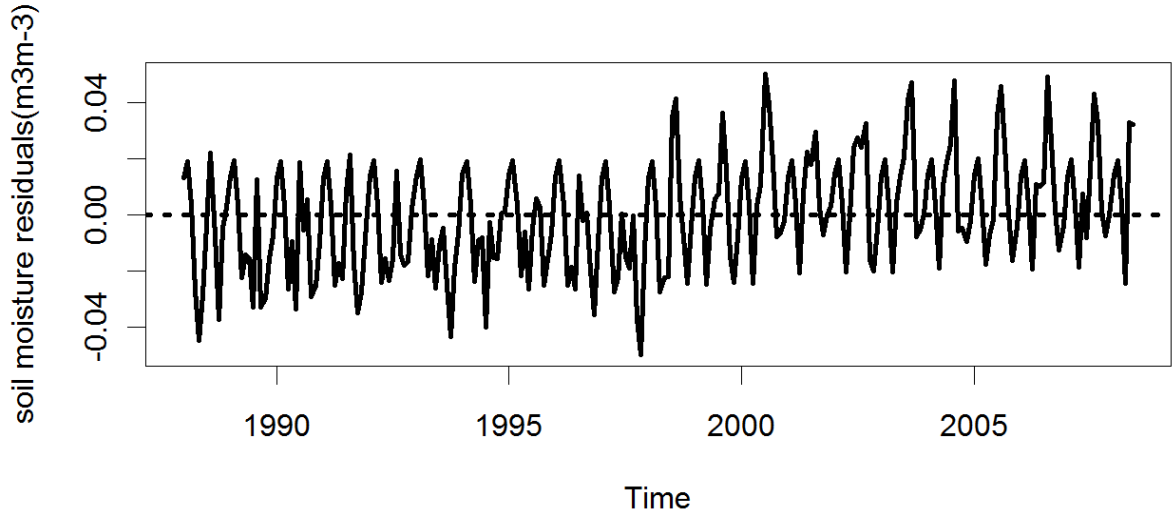


Figure 23: soil moisture residuals after eliminating periodicity (location 16)

The residual plots of the periodic functions of LST and soil moisture clearly indicate that the seasonal signals have been removed. However, the plots are not stationary. For the soil moisture residual plot, the variance is not constant. See figure 23 above. Therefore, first order differencing to eliminate trend and stabilize the variance of the residual data was performed (Castellano-Méndez, González-Manteiga et al. 2004). The general model for first order differencing is given by;

$$\nabla Z_t = Z_t - Z_{t-1} \quad [33]$$

For a given time series with a linear trend of the form;

$$Z_t = \beta_0 + \beta_1 t + \varepsilon_t, \quad [34]$$

application of differencing results in a time series with a constant mean, hence stationary time series.

$$\begin{aligned} \nabla Z_t &= (\beta_0 + \beta_1 t + \varepsilon_t) - (\beta_0 + \beta_1 (t-1) + \varepsilon_{t-1}) \\ \nabla Z_t &= \beta_1 + \varepsilon_t - \varepsilon_{t-1} \end{aligned} \quad [35]$$

Where ∇Z is the differenced time series variable, β_0 is the intercept, β_1 is the slope, ε is the random error and t is the time of measurement

The differenced stationary residual plots of LST and soil moisture are illustrated in the figures 24 and 25 respectively. The figures clearly demonstrate a stationary time series with a constant mean and constant variance apart from where there are possible breaks in the series.

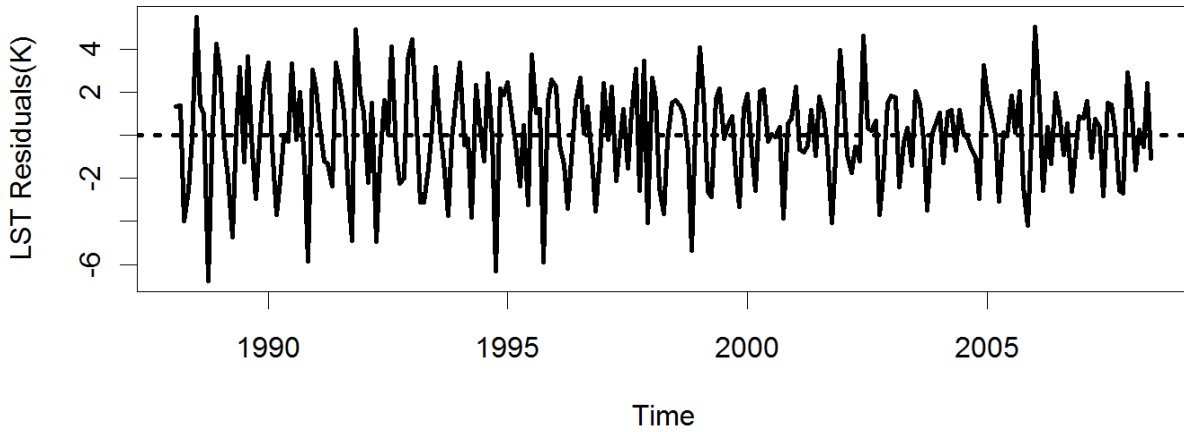


Figure 24: Land surface temperature residuals after removing both periodicity and trend (location 12)

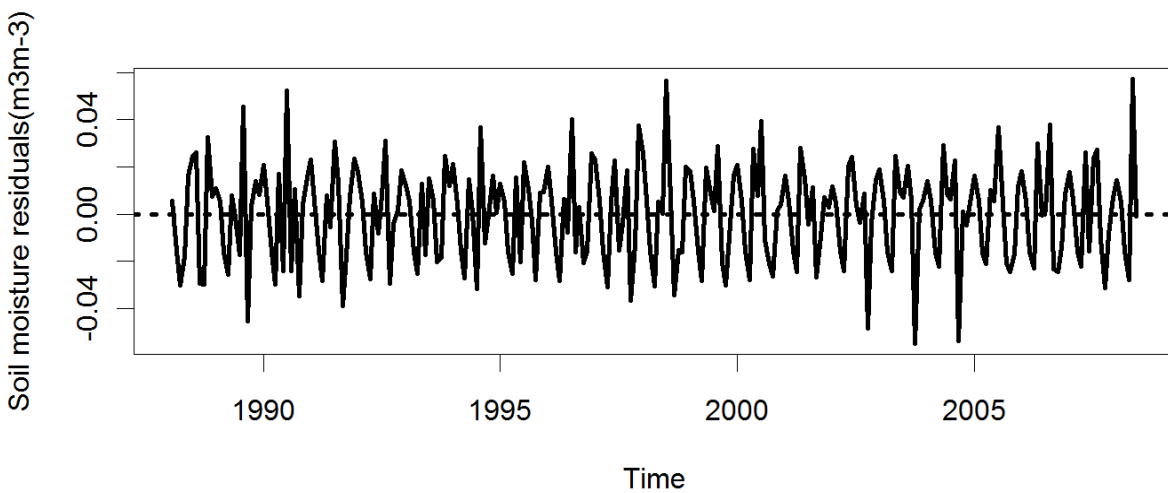


Figure 25: soil moisture residuals after removing both periodicity and trend (location 16)

The auto correlation and partial auto correlation functions of the stationary residuals were plotted to identify the ARIMA models that describe soil moisture and LST over the Tibetan plateau. This procedure was repeated for 20 randomly selected pixels and the result is summarized in the table 7 below. Three possible models emerged from this preliminary test i.e. ARIMA(0,1,1), ARIMA(1,1,0) and ARIMA(1,1,1). These three models were then used as a guide for an automatic ARIMA model fitting (Hyndman and Koehler 2006; Hyndman and Khandakar 2008). This does not only reveal the seasonal component of model parameters but it also eliminates any subjective decision which could have been made when selecting the model orders. The clear sine wave appearing on the ACF plot in the figure 26 below, is an indication that, there is a seasonal AR component in the time series

Table 7: ARIMA models for LST and soil moisture derived from the analysis of ACF and PACF

Loc No	Lat	Lon	model	order	model	order
			Soil moisture		LST	
1	30° 14'N	92° 00'E	ARIMA	(0,1,1)	ARIMA	(0,1,1)
2	36° 20'N	94° 30'E	ARIMA	(1,1,1)	ARIMA	(1,1,1)
3	34° 05'N	99° 58'E	ARIMA	(1,1,1)	ARIMA	(1,1,1)
4	38° 05'N	102° 36'E	ARIMA	(1,1,0)	ARIMA	(1,1,1)
5	35° 05'N	103° 26'E	ARIMA	(1,1,1)	ARIMA	(1,1,1)
6	30° 05'N	98° 13'E	ARIMA	(0,1,1)	ARIMA	(0,1,1)
7	28° 11'N	87° 14'E	ARIMA	(1,1,1)	ARIMA	(1,1,1)
8	31° 53'N	84° 34'E	ARIMA	(1,1,1)	ARIMA	(1,1,1)
9	34° 38'N	84° 48'E	ARIMA	(1,1,0)	ARIMA	(1,1,1)
10	37° 17'N	83° 54'E	ARIMA	(1,1,1)	ARIMA	(1,1,1)
11	39° 29'N	88° 55'E	ARIMA	(1,1,0)	ARIMA	(1,1,1)
12	37° 44'N	93° 40'E	ARIMA	(0,1,1)	ARIMA	(1,1,1)
13	36° 17'N	95° 02'E	ARIMA	(1,1,1)	ARIMA	(1,1,1)
14	33° 41'N	92° 04'E	ARIMA	(1,1,1)	ARIMA	(1,1,1)
15	29° 59'N	87° 21'E	ARIMA	(1,1,1)	ARIMA	(1,1,1)
16	34° 17'N	89° 03'E	ARIMA	(1,1,0)	ARIMA	(1,1,1)
17	31° 05'N	90° 46'E	ARIMA	(1,1,1)	ARIMA	(1,1,1)
18	33° 14'N	93° 43'E	ARIMA	(1,1,0)	ARIMA	(0,1,1)
19	32° 14'N	97° 10'E	ARIMA	(1,1,0)	ARIMA	(1,1,1)
20	35° 41'N	94° 35'E	ARIMA	(1,1,1)	ARIMA	(1,1,1)

Three final suitable ARIMA models that emerged out of the automatic ARIMA model fitting are ; ARIMA(0,1,1) (2,0,0)₁₂ ,ARIMA(1,1,0) (2,0,0)₁₂ and ARIMA (1,1,1) (2,0,0)₁₂. The ACF and PACF plots demonstrated a mixture of AR and MA process for different pixels. See figures 26 and 27 below.

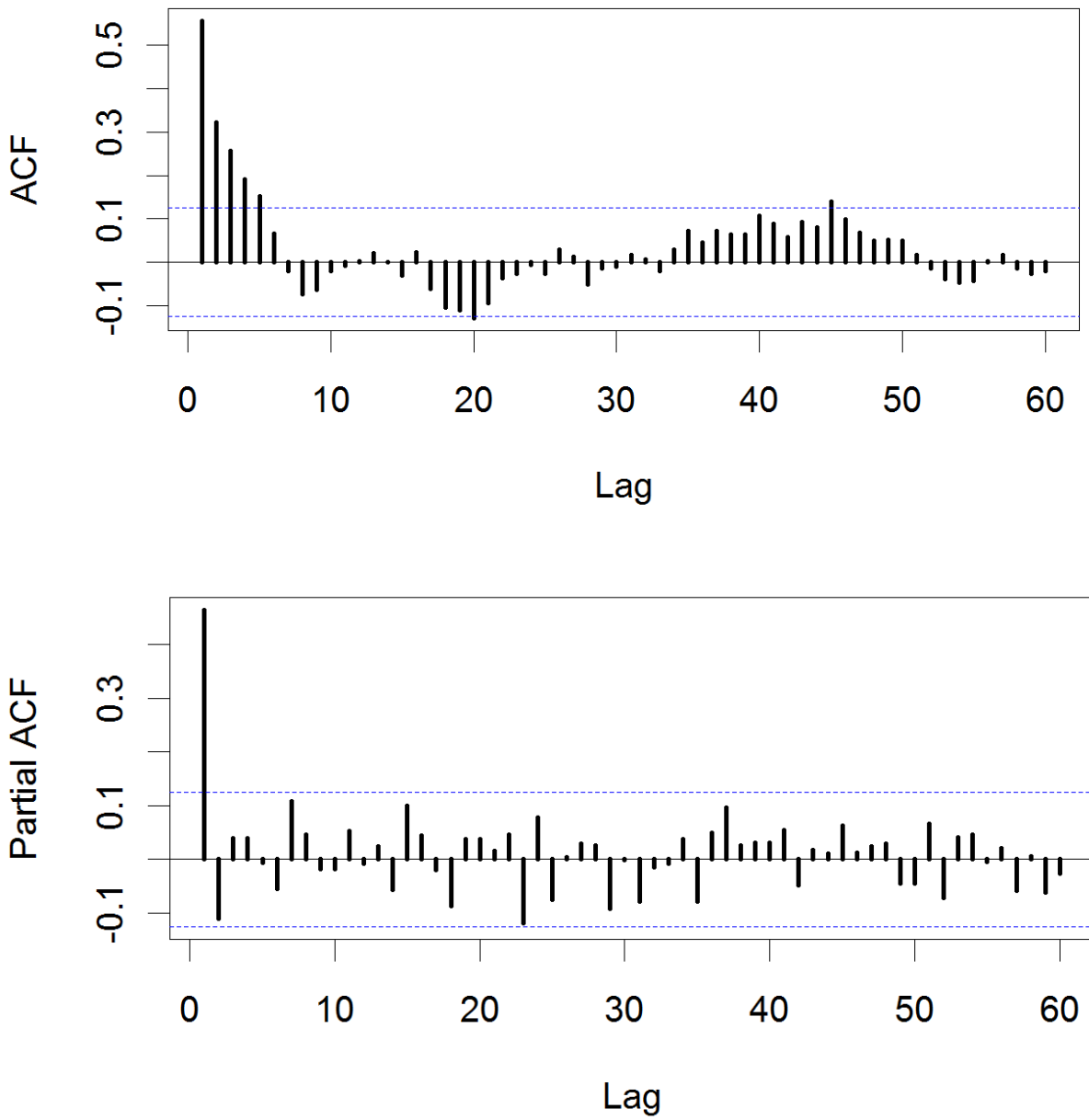


Figure 26: ACF and PACF plots demonstrating a clear AR process of LST at location 12

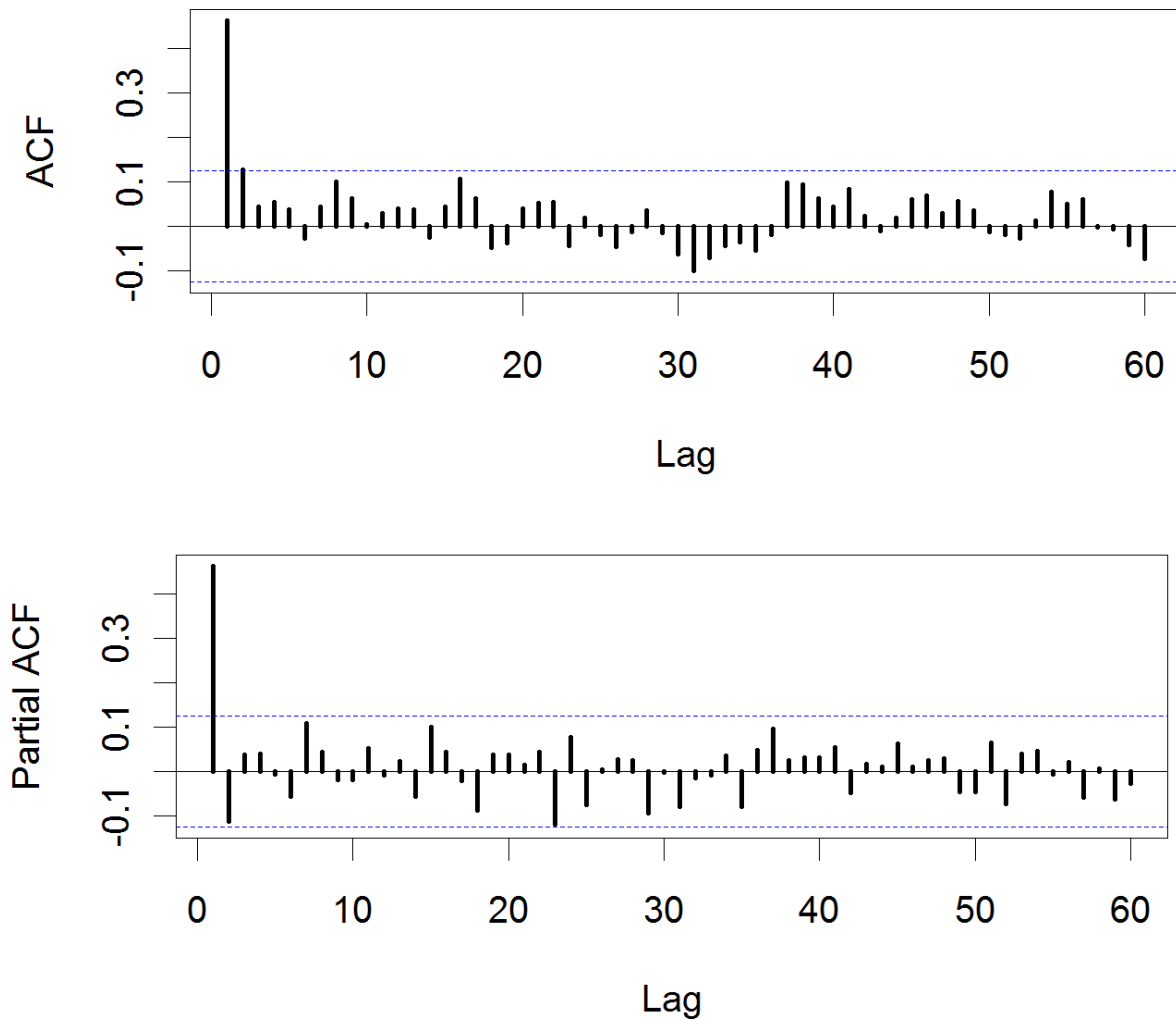


Figure 27: ACF and PACF plots demonstrating a case of a MA and AR process of soil moisture at location 16. Note; the dotted blue line represents the 95% confidence limits

The ACF plot in figure 26 above attenuates at the low lags up to 5, indicating that the process can be modelled as an AR process and the PACF in the same figure truncates at the first lag suggesting that the order of the AR process is 1. The seasonal AR (sAR) derived from Automatic ARIMA fitting is 2. Recall that the residuals were differenced once. Therefore, for this location the ARIMA model is written as $ARIMA(1, 1, 0)(2, 0, 0)_{12}$. However, in figure 27 the ACF truncates at the first lag indicating that the process can be modelled as a MA and the PACF in the same figure also truncates at the first lag, suggesting that the model incorporates an AR process. In both cases the model order is 1, the residuals were differenced once and the sAR is 2. Therefore, for this location the ARIMA model is written as $ARIMA(1,1,1)(2,0,0)_{12}$ (Piwowar and Ledrew 2002; Yurekli and Kurunc 2006). Similar results were obtained for all the remaining 19 locations for both soil moisture and LST time series.

8.3. Model estimation (fitting)

The above three identified suitable models were fitted to the time series data and the model parameters were estimated. See tables 8 and 9 for soil moisture and LST respectively. The most parsimonious model based on the lowest Akaike Information Criterion (AIC) was evaluated further, for the goodness of fit through the analysis of residual ACF (Akaike 1974; Kim and Kim 2007; Yürekli, Simsek et al. 2007). A well fitted model removes all auto correlation from model residuals and the residual autocorrelations should not be significantly different from zero. See figures 28 and 29 below for soil moisture and LST respectively. Further diagnostic evaluation included test of significance of the parameter estimates and variance of the residuals. The parameters greater than twice their standard error are significant at 95% confidence level (Piwowar and Ledrew 2002).

$$AIC(m) = n \ln \sigma_a^2 + 2m \quad [36]$$

Where m is the sum of AR and MA orders, n is the length of the time series and σ_a^2 is the residual variance

Table 8: Comparison of suitable ARIMA models for soil moisture

Model	Parameter	Estimate	Std error	variance	AIC
ARIMA(1,1,0)(2,0,0)	AR1	-0.3063	0.0629		
	sAR1	0.5005**	0.0582		
	sAR2	0.4520**	0.0591	0.00028	-1269.68
ARIMA(0,1,1)(2,0,0)	MA1	-0.3961	0.0891		
	sAR1	0.4464**	0.0566		
	sAR2	0.4935**	0.0592	0.00064	-1053.83
ARIMA(1,1,1)(2,0,0)	AR1	0.5881**	0.0545		
	MA1	-1.000	0.00076		
	sAR1	0.4328**	0.0569		
	sAR2	0.4869**	0.0592	0.00056	-1086.83

** implies significant at 95% confidence level

Table 9: comparison of suitable ARIMA models for LST

Model	Parameter	Estimate	Std error	variance	AIC
ARIMA(1,1,0)(2,0,0)	AR1	-0.2578	0.0646		
	sAR1	0.4539**	0.0551		
	sAR2	0.4977**	0.0565	8.358	1250.72
ARIMA(0,1,1)(2,0,0)	MA1	-0.7694	0.0787		
	sAR1	0.4670**	0.0546		
	sAR2	0.5162**	0.0553	7.246	1228.95
ARIMA(1,1,1)(2,0,0)	AR1	0.4749**	0.0602		
	MA1	-1.000	0.0071		
	sAR1	0.4847**	0.0565		
	sAR2	0.4796**	0.0571	6.594	1197.29

** implies significant at 95% confidence level

8.4. Model verification (validation)

Model verification was done through the comparison of the modelled land surface temperature and soil moisture to the satellite derived time series. The coefficient of determination was 94 for soil moisture and 95 for LST. A split sample forecasting was done for both soil moisture and LST time series. The forecast was generated by fitting the suitable models to the first 228 months. This model was then used to forecast the remaining 18 months and the forecasting accuracy assessed (Hyndman and Koehler 2006; Hyndman and Khandakar 2008). Table 10 summarises the results of forecasting. Both the observed and simulated values were within the 95% confidence interval, therefore the model is considered to be valid (Young and Minchin 1991; Piwowar and Ledrew 2002; Romilly 2005). Figures 30 and 31 below show how far into the future soil moisture and LST temperature can be forecast within 80% and 95% confident limits. For soil moisture, the uncertainty band widens significantly within 18 months while the uncertainty band for LST remains relatively stable for over 5 years with a systematic decline.

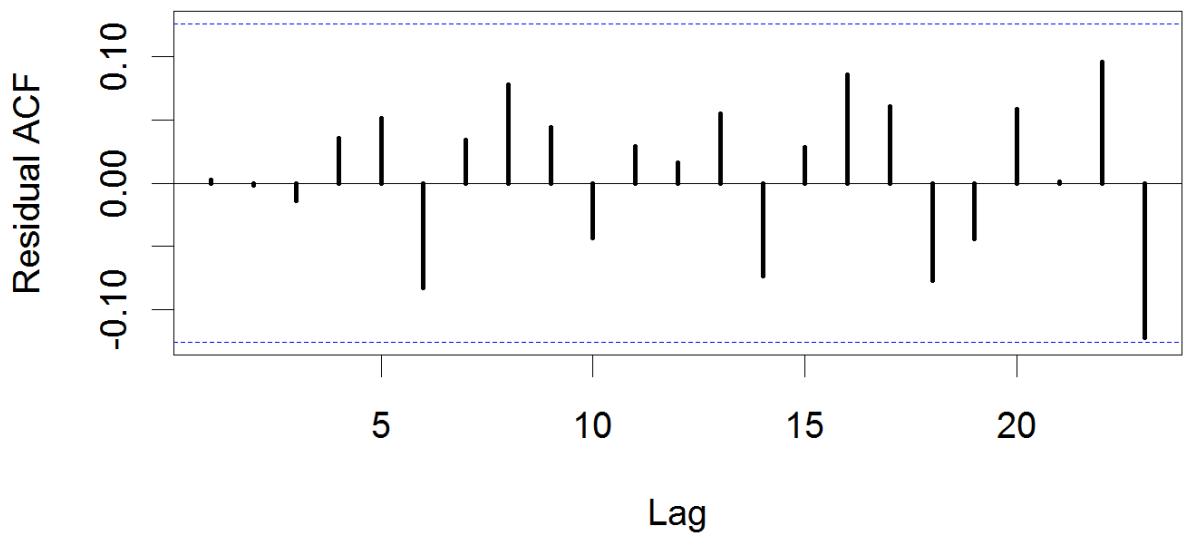


Figure 28: ACF plot of fitted LST residuals

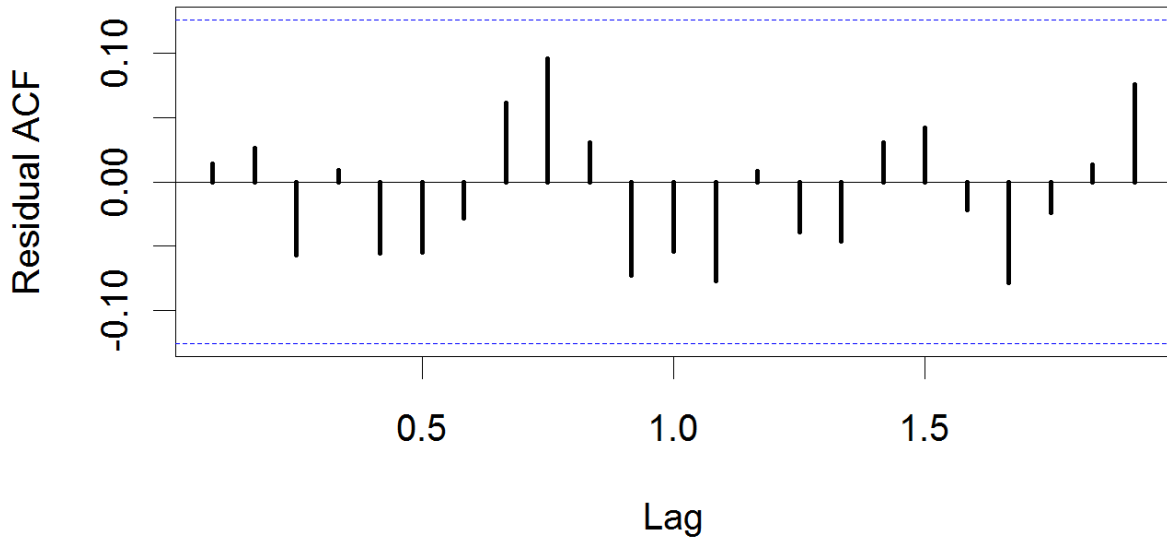


Figure 29: ACF plot of fitted soil moisture residuals

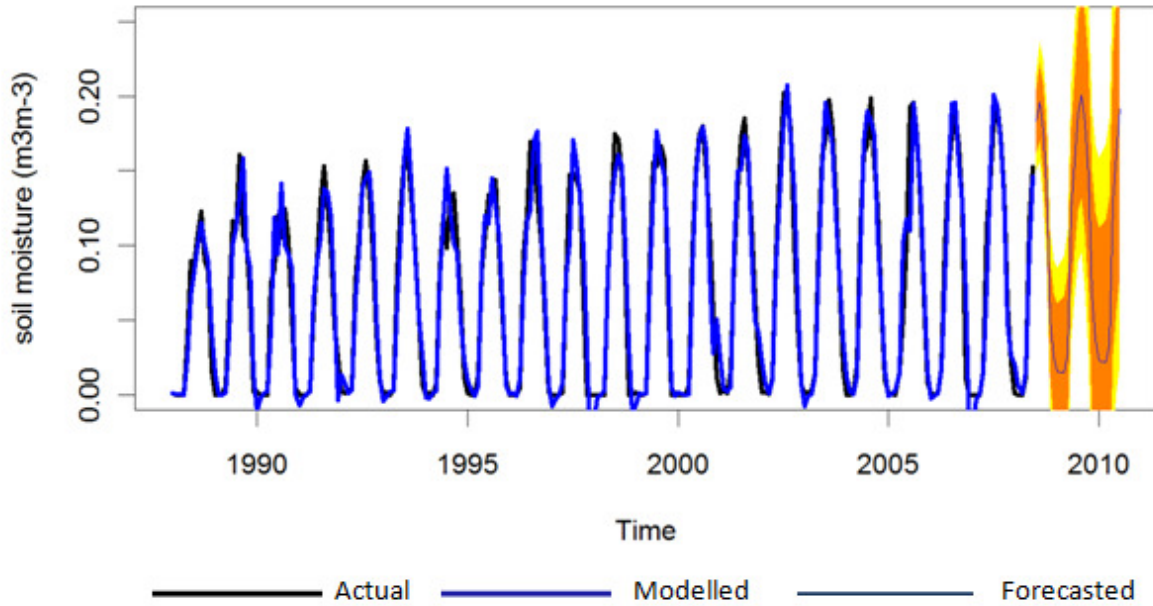


Figure 30: Long term forecasting of soil moisture at location 16

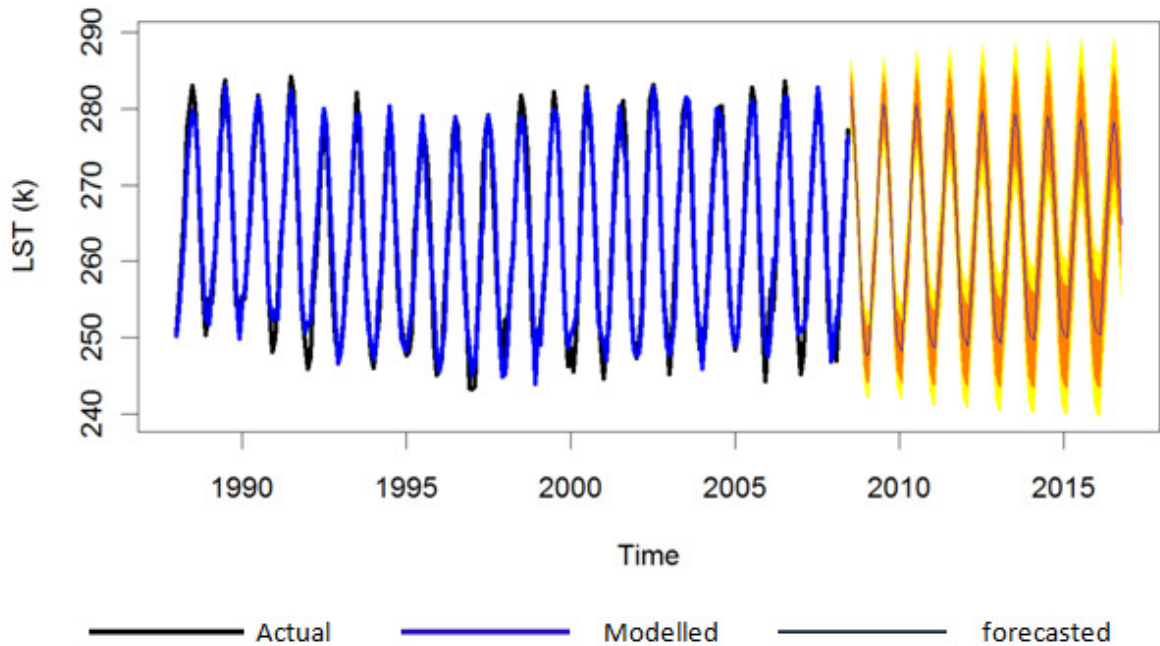


Figure 31: long term forecasting of Land surface temperature at location 12

Note: the yellow areas represent 95% confident limits while the orange areas represent the 80% confident limits.

Table 10: Summary of soil moisture and LST forecasting accuracy

Variable	R ²	ME	RMSE	MAE
Soil moisture	0.94	-0.033	0.045	0.033
LST	0.95	2.323	3.052	2.323

ME=mean error, RMSE= root mean square error, MAE=Mean absolute error

In summary, the results of the analysis of the ACF and PACF plots of the fitted models and the comparison of the AIC of the competing models, suggest that soil moisture can be modelled as $ARIMA(1,1,0)(2,0,0)_{12}$ while the LST can be modelled as $ARIMA(1,1,1)(2,0,0)_{12}$. Diagnostic evaluation of the residuals of the fitted models indicated that the residuals were normally distributed with a mean of zero. The residual ACF plot of LST was generally not significantly different from zero. However, some of the residual ACF plot of soil moisture had significant residuals around multiple of 12 suggesting that there is some unexplained variation in the time series. A forecast of both LST and soil moisture provided valid results with an error of $0.045\text{m}^3\text{m}^{-3}$ for soil moisture and 3K for LST time series.

9. Summary and Conclusions

An algorithm for the retrieval of soil moisture, LST and vegetation transmissivity from the observed brightness temperatures, of the dual polarized 19GHz and 37GHz V- polarized channels of SSM/I, has been applied to retrieve surface variables over the Tibetan plateau. The advantage of this algorithm over other similar algorithms is that, it does not require soil parameters such as soil texture, soil porosity, wilting point or vegetation parameters such as vegetation water content. Soil parameters have insignificant contribution to the total error in soil moisture retrieval (deJeu 2003).

Two assumptions were made in this algorithm; the first assumption was that atmospheric effect on both 19 and 37GHz channels were negligible and the second assumption was that canopy temperature is equal to soil temperature. However, to ensure the second assumption holds true, the SSM/I data for the descending pass of satellites F11 and F13 and the ascending pass of F08 were used in this study. This is because at this time of the day (6:30AM), thermodynamic temperature is relatively stable compared to during afternoon hours and therefore soil temperature can be assumed to be equal to canopy temperature.

A constant value of single scattering albedo and two sets of surface roughness parameters (i.e. 0.05cm for winter and 0.0cm for the rest of the year) were used based on literature and after a validation process to identify suitable parameters for the Tibetan plateau. This study revealed that for the Tibetan plateau surface roughness parameter value of 0.0cm is the most appropriate for soil moisture retrieval. However, the influence of frozen soils on soil moisture retrieval was accounted for by calibrating the roughness parameter during the winter time. This was to counteract the influence of increased emissivity and therefore increased brightness temperature caused by freezing, which impedes the ability of water molecules to rotate.

The retrieved vegetation transmissivity showed seasonal variation with the highest value occurring during the peak of winter and the lowest value occurring during the peak of summer. This is expected because, during the peak of winter, nearly all of the vegetation will have shed off their leaves, hence a higher transparency to microwave emission. On the other hand during the peak of summer nearly all the vegetation have full grown vegetation canopy and therefore less transparent to the microwave emission.

Soil moisture retrieval using the dual polarized 19GHz and the V-polarized 37GHz channels of the SSM/I is sensitive to the 19GHz and 37GHz vertical polarizations while vegetation transmissivity is sensitive to the 19GHz vertical and horizontal polarization frequencies. The time series of both the retrieved land surface temperature and soil moisture are in good agreement with the measured land surface temperature and soil moisture with an error of ± 2.87 K and ± 0.04 m³m⁻³ for the land surface temperature and soil moisture respectively.

The entire TP experienced significant warming over the last two decades except the water bodies. However, the central TP experienced more significant positive trend in land surface temperature anomalies. A similar trend is observed over scattered areas in the east and northern part of TP. while the south and south eastern part of the TP experienced the least changes in temperature anomalies. The magnitude of warming over the TP is in the range of 0.2°C to 1.1°C/decade. Warming was more

paramount at elevations over 3000m above sea level compared to areas with elevation below 3000m above sea level. The western and northern part of the TP experienced an increasing significant trend in mean annual soil moisture anomalies. While the eastern and south eastern part of the TP showed no trend in soil moisture anomalies. The soil moisture anomalies over the TP increased at the rate of 0.03 to 0.13% (volume/volume) per year. The annual trend was highest during the summer monsoon season than during the winter season.

LST and soil moisture are crucial in surface energy balance and control of climate feedback mechanism. While LST is well represented in general circulation models (GCMs), there is need to better represent soil moisture in the GCMs to improve their performance. Besides the inclusion of soil moisture in GCMs, prior knowledge of future soil moisture is a prerequisite for better agricultural planning. One of the best ways to understand a stochastic process is to model it. Therefore the time series of both LST and soil moisture were modelled using ARIMA family of time series analysis. As would be expected both LST and soil moisture exhibit strong seasonal characteristics with maximum values being registered in June - July and the minimum values in December – January. ARIMA models were fitted to the data after both the trend and the seasonal components had been removed. Following the analysis of ACF and PACF plots of the fitted models and the comparison of the AIC of the competing models, it is apparent that soil moisture can be modelled as $ARIMA(1,1,0)(2,0,0)_{12}$ while the LST can be modelled as $ARIMA(1,1,1)(2,0,0)_{12}$. Diagnostic evaluation of the residuals of the fitted models indicated that the residuals were normally distributed with a mean of zero. The residual ACF plot of LST was generally not significantly different from zero. However, some of the residual ACF plot of soil moisture had significant residuals around multiple of 12 suggesting that there is some unexplained variation in the time series. A forecast of both LST and soil moisture provided valid results with an error of $0.045\text{m}^3\text{m}^{-3}$ for soil moisture and 3K for LST time series, therefore forecasting using ARIMA model could provide climate models with the needed soil moisture inputs.

10. References:

- Akaike, H. (1974). "A new look at the statistical model identification." IEEE Transactions on Automatic Control **19**(6): 716-723.
- Alec Sithole, C. T. F. M. (2009). "Climate variability and change over southern Africa: impacts and challenges." African Journal of Ecology **47**(s1): 17-20.
- Bindlish, R., T. J. Jackson, et al. (2008). "Aircraft based soil moisture retrievals under mixed vegetation and topographic conditions." Remote Sensing of Environment **112**(2): 375-390.
- Bindlish, R., T. J. Jackson, et al. (2003). "Soil moisture estimates from TRMM Microwave Imager observations over the Southern United States." Remote Sensing of Environment **85**(4): 507-515.
- Bown, F. and A. Rivera (2007). "Climate changes and recent glacier behaviour in the Chilean Lake District." Global and Planetary Change **59**(1-4): 79-86.
- Boyles, R. P. and S. Raman (2003). "Analysis of climate trends in North Carolina (1949-1998)." Environment International **29**(2-3): 263-275.
- Brockwell, P. J. and R. A. Davis, Eds. (1996). Introduction to Time Series and Forecasting. New York., Springer-Verlag.
- Castellano-Méndez, M., W. González-Manteiga, et al. (2004). "Modelling of the monthly and daily behaviour of the runoff of the Xallas river using Box-Jenkins and neural networks methods." Journal of Hydrology **296**(1-4): 38-58.
- Chatfield, C., Ed. (2003). The analysis of time series: An introduction. Boca Raton London New York Washington, D.C., Chapman and Hall/ CRC.
- Choudhury, B. J., T. J. Schmugge, et al. (1979). "Effect of surface roughness on microwave emission of soils." Journal of Geophysical Research, **84**: 5699-5706.
- Cimino, G., G. Del Duce, et al. (1999). "Time series analysis of geological data." Chemical Geology **161**(1-3): 253-270.
- Dash, P., F. M. Gottsche, et al. (2002). "Land surface temperature and emissivity estimation from passive sensor data: theory and practice-current trends." International Journal of Remote Sensing **23**(13): 2563-2594.
- de Beurs, K. M. and G. M. Henebry (2005). "A statistical framework for the analysis of long image time series." International Journal of Remote Sensing **26**(8): 1551-1573.
- De Ridder, K. (2003). "Surface soil moisture monitoring over Europe using Special Sensor Microwave/Imager (SSM/I) imagery." Journal of Geophysical Research-Atmospheres **108**(D14).
- deJeu, R. (2003). Retrieval of land surface parameters using passive microwave remote sensing. Amsterdam, Vrije Universiteit. **PhD Thesis**.

- Dobson, M. C., F. T. Ulaby, et al. (1985). "Microwave Dielectric Behavior of Wet Soil-Part II: Dielectric Mixing Models." IEEE Transactions on Geoscience and Remote Sensing **GE-23**(1): 35-46.
- Draper, C. S., J. P. Walker, et al. (2009). "An evaluation of AMSR-E derived soil moisture over Australia." Remote Sensing of Environment **113**(4): 703-710.
- Drusch, M., E. F. Wood, et al. (2001). "Vegetative and atmospheric corrections for the soil moisture retrieval from passive microwave remote sensing data: Results from the Southern Great Plains Hydrology Experiment 1997." Journal of Hydrometeorology **2**(2): 181-192.
- Ford, C. R., C. E. Goranson, et al. (2005). "Modeling canopy transpiration using time series analysis: A case study illustrating the effect of soil moisture deficit on *Pinus taeda*." Agricultural and Forest Meteorology **130**(3-4): 163-175.
- Fu, C., Z. Jiang, et al. (2008). Effects of the Tibetan Plateau on the Climate of China. Regional Climate Studies of China, Springer: 219-270.
- G.C.Topp, J.L.Davis, et al. (1980). "Electromagnetic Determination of Soil Water Content: Measurements in Coaxial Transmission Lines." Water Resources Research **16**(3): 574-582.
- Gao, H., E. F. Wood, et al. (2006). "Using TRMM/TMI to retrieve surface soil moisture over the southern United States from 1998 to 2002." Journal of Hydrometeorology **7**(1): 23-38.
- Hallikainen, M. T., F. T. Ulaby, et al. (1985). "Microwave Dielectric Behavior of Wet Soil-Part I: Empirical Models and Experimental Observations." IEEE Transactions on Geoscience and Remote Sensing **GE-23**(1): 25-34.
- Herzschuh, U., A. Kramer, et al. (2009). "Quantitative climate and vegetation trends since the late glacial on the northeastern Tibetan Plateau deduced from Koucha Lake pollen spectra." Quaternary Research **71**(2): 162-171.
- Hipel, W. K. and A. I. Mcleod, Eds. (1994). Time Series Modelling of Water Resources and Environmental Systems. Amsterdam, Elsevier.
- Hollinger, J., R. Lo, et al., Eds. (1987). Special Sensor Microwave/Imager's users guide, NRL Tech. Rep., Washington, DC, Naval Research Laboratory. 177 pp.
- Holmes, T. R. H., R. A. M. de Jeu, et al. (2009). "Land surface temperature from Ka band (37 GHz) passive microwave observations." Journal of Geophysical Research-Atmospheres **114**.
- Hyndman, R. J. and Y. Khandakar (2008). "Automatic time series forecasting: The forecast package for R." Journal of Statistical Software **27**(3): 1 - 21.
- Hyndman, R. J. and A. B. Koehler (2006). "Another look at measures of forecast accuracy." International Journal of Forecasting **22**(4): 679-688.
- Jackson, T. J. (1997). "Soil Moisture Estimation using Special Satellite Microwave/Imager Satellite Data Over a Grassland Region." Water Resources Research. **33**: 1475 - 1484.
- Jackson, T. J., A. Y. Hsu, et al. (2002). "Surface soil moisture retrieval and mapping using high-frequency microwave satellite observations in the Southern Great Plains." Journal of Hydrometeorology **3**(6): 688-699.

- Kärner, O. (2009). "ARIMA representation for daily solar irradiance and surface air temperature time series." Journal of Atmospheric and Solar-Terrestrial Physics **71**(8-9): 841-847.
- Katz, R. W. and B. G. Brown (1992). "Extreme events in a changing climate - variability is more important than averages." Climatic Change **21**(3): 289-302.
- Kerr, Y. H. and E. G. Njoku (1990). "A semiempirical model for interpreting microwave emission from semiarid land surfaces as seen from space." IEEE Transactions on Geoscience and Remote Sensing **28**(3): 384-393.
- Kim, S. and H. Kim (2007). "Stochastic analysis of soil moisture to understand spatial and temporal variations of soil wetness at a steep hillside." Journal of Hydrology **341**(1-2): 1-11.
- Krishna Prasad, V., K. V. S. Badarinath, et al. (2007). "Spatial patterns of vegetation phenology metrics and related climatic controls of eight contrasting forest types in India – analysis from remote sensing datasets." Theoretical and Applied Climatology **89**(1): 95-107.
- Latifovic, R. and D. Pouliot (2007). "Analysis of climate change impacts on lake ice phenology in Canada using the historical satellite data record." Remote Sensing of Environment **106**(4): 492-507.
- Lee, K.-H. and E. N. Anagnostou (2004). "A combined passive/active microwave remote sensing approach for surface variable retrieval using Tropical Rainfall Measuring Mission observations." Remote Sensing of Environment **92**(1): 112-125.
- Li, Y., E. P. Campbell, et al. (2003). "Statistical forecasting of soil dryness index in the southwest of Western Australia." Forest Ecology and Management **183**(1-3): 147-157.
- Liu, J., S. Wang, et al. (2009). "Climate warming and growth of high-elevation inland lakes on the Tibetan Plateau." Global and Planetary Change **67**(3-4): 209-217.
- Liu, X. and B. Chen (2000). "Climatic warming in the Tibetan Plateau during recent decades." International Journal of Climatology **20**(14): 1729-1742.
- Liu, X., Z. Cheng, et al. (2009). "Elevation dependency of recent and future minimum surface air temperature trends in the Tibetan Plateau and its surroundings." Global and Planetary Change **68**(3): 164-174.
- Liu, Y. Y., A. van Dijk, et al. (2009). "An analysis of spatiotemporal variations of soil and vegetation moisture from a 29-year satellite-derived data set over mainland Australia." Water Resources Research **45**.
- Löscher, A., C. Retscher, et al. (2008). "Variational optimization for global climate analysis on ESA's high performance computing grid." Remote Sensing of Environment **112**(4): 1450-1463.
- Magagi, R. D. and Y. H. Kerr (2001). "Estimating surface soil moisture and soil roughness over semiarid areas from the use of the copolarization ratio." Remote Sensing of Environment **75**(3): 432-445.
- Maslanik, J. and J. Stroeve (2009). "DMSP SSM/I daily polar gridded brightness temperatures, 1987 - 2008." Boulder, CO: National Snow and Ice Data Center. Digital media.

- Matondo, J. I., G. Peter, et al. (2004). "Evaluation of the impact of climate change on hydrology and water resources in Swaziland: Part I." Physics and Chemistry of the Earth, Parts A/B/C **29**(15-18): 1181-1191.
- McFarland, M. J., R. L. Miller, et al. (1990). "Land surface temperature derived from the SSM/I passive microwave brightness temperatures." IEEE Transactions on Geoscience and Remote Sensing **28**(5): 839-845.
- Mikhail, E. M., Ed. (1976). Observations and Least Squares. University Press of America. New York (497pp).
- Mo, T., B. J. Choudhury, et al. (1982). "A model for microwave emission from vegetation-covered fields." Journal of Geophysical Research **87**(11): 229-237.
- Morland, J. C., D. I. F. Grimes, et al. (2001). "Satellite observations of the microwave emissivity of a semi-arid land surface." Remote Sensing of Environment **77**(2): 149-164.
- Nagai, S., K. Ichii, et al. (2007). "Interannual variations in vegetation activities and climate variability caused by ENSO in tropical rainforests." International Journal of Remote Sensing **28**(6): 1285-1297.
- Njoku, E. G. and S. K. Chan (2006). "Vegetation and surface roughness effects on AMSR-E land observations." Remote Sensing of Environment **100**(2): 190-199.
- Owe, M., R. de Jeu, et al. (2001). "A methodology for surface soil moisture and vegetation optical depth retrieval using the microwave polarization difference index." IEEE Transactions on Geoscience and Remote Sensing **39**(8): 1643-1654.
- Panciera, R., J. P. Walker, et al. (2009). "Evaluation of the SMOS L-MEB passive microwave soil moisture retrieval algorithm." Remote Sensing of Environment **113**(2): 435-444.
- Piwowar, J. M. and E. F. Ledrew (2002). "ARMA time series modelling of remote sensing imagery: a new approach for climate change studies." International Journal of Remote Sensing **23**(24): 5225-5248.
- Puatanachokchai, C. and E. M. Mikhail (2008). "Adjustability and error propagation for true replacement sensor models." Isprs Journal of Photogrammetry and Remote Sensing **63**(3): 352-364.
- Raynolds, M. K., J. C. Comiso, et al. (2008). "Relationship between satellite-derived land surface temperatures, arctic vegetation types, and NDVI." Remote Sensing of Environment **112**(4): 1884-1894.
- Romilly, P. (2005). "Time series modelling of global mean temperature for managerial decision-making." Journal of Environmental Management **76**(1): 61-70.
- Sandells, M. J., I. J. Davenport, et al. (2008). "Passive L-band microwave soil moisture retrieval error arising from topography in otherwise uniform scenes." Advances in Water Resources **31**(11): 1433-1443.
- Shi, W., C.-K. Cheung, et al. (2004). "Modelling error propagation in vector-based overlay analysis." Isprs Journal of Photogrammetry and Remote Sensing **59**(1-2): 47-59.

- Slini, T., K. Karatzas, et al. (2002). "Statistical analysis of environmental data as the basis of forecasting: an air quality application." The Science of The Total Environment **288**(3): 227-237.
- Tan, S. Y. (2007). "The influence of temperature and precipitation climate regimes on vegetation dynamics in the US Great Plains: A satellite bioclimatology case study." International Journal of Remote Sensing **28**(22): 4947-4966.
- Tao, F., M. Yokozawa, et al. (2008). "Land surface phenology dynamics and climate variations in the North East China Transect (NECT), 1982-2000." International Journal of Remote Sensing **29**(19): 5461-5478.
- Trenberth, K. E., P. D. Jones, et al. (2007). Observations: Surface and Atmospheric Climate Change. In: *Climate Change 2007: The Physical Science Basis*. Contribution of Working Group I to the Fourth Assessment Report of the Intergovernmental Panel on Climate Change. S. Solomon, D. Qin, M. Manning, Z. Chen, M. Marquis, K.B. Averyt, M. Tignor and H.L. Miller (eds). Cambridge University Press, Cambridge, United Kingdom and New York, NY, USA.
- Ulaby, F. T., R. Moore, et al., Eds. (1981). Microwave remote sensing: Active and Passive. Fundamentals and radiometry. Boston, MA, Addison Wesley.
- Van de Griend, A. A. and M. Owe (1993). "Determination of microwave vegetation optical depth and single scattering albedo from large-scale soil-moisture and Nimbus SMMR satellite-observations " International Journal of Remote Sensing **14**(10): 1875-1886.
- van de Griend, A. A. and M. Owe (1994). "The influence of polarization on canopy transmission properties at 6.6 GHz and implications for large scale soil moisture monitoring in semi-arid environments." IEEE Transactions on Geoscience and Remote Sensing **32**(2): 409-415.
- van de Griend, A. A., M. Owe, et al. (1996). "Measurement and behavior of dual-polarization vegetation optical depth and single scattering albedo at 1.4- and 5-GHz microwave frequencies." IEEE Transactions on Geoscience and Remote Sensing **34**(4): 957-965.
- Verbesselt, J., R. Hyndman, et al. (2009). "Detecting trend and seasonal changes in satellite image time series." Remote Sensing of Environment **114**(1): 106-115.
- Vinnikov, K. Y. and A. Robock (2002). "Trends in moments of climatic indices." Geophysical Research Letters **29**(2): 14 -1 14 - 4.
- Vinnikov, K. Y., A. Robock, et al. (2002). "Diurnal and seasonal cycles of trends of surface air temperature." Journal of Geophysical Research-Atmospheres **107**(D22): ACL 13 -1 ACL 13 - 9.
- Wang, J. R. (1985). "Effect of vegetation on soil moisture sensing observed from orbiting microwave radiometers." Remote Sensing of Environment **17**(2): 141-151.
- Wang, J. R. and B. J. Choudhury (1981). "Remote sensing of soil moisture content over bare field at 1.4GHz frequency." Journal of Geophysical Research **86**: 5277-5282.
- Wang, J. R. and T. J. Schmugge (1980). "An Empirical Model for the Complex Dielectric Permittivity of Soils as a Function of Water Content." IEEE Transactions on Geoscience and Remote Sensing **GE-18**(4): 288-295.

- Wegmüller, U. (1990). "The effect of freezing and thawing on the microwave signatures of bare soil." Remote Sensing of Environment **33**(2): 123-135.
- Wen, J., T. J. Jackson, et al. (2005). "Retrieval of soil moisture and vegetation water content using SSM/I data over a corn and soybean region." Journal of Hydrometeorology **6**(6): 854-863.
- Wen, J., Z. Su, et al. (2003). "Determination of land surface temperature and soil moisture from Tropical Rainfall Measuring Mission/Microwave Imager remote sensing data." Journal of Geophysical Research **108**(2): ACL 2-1 ACL 2-10.
- Weng, F. Z. and N. C. Grody (1998). "Physical retrieval of land surface temperature using the special sensor microwave imager." Journal of Geophysical Research-Atmospheres **103**(D8): 8839-8848.
- Wigneron, J. P., J. C. Calvet, et al. (2003). "Retrieving near-surface soil moisture from microwave radiometric observations: current status and future plans." Remote Sensing of Environment **85**(4): 489-506.
- Young, P. C. and P. E. H. Minchin (1991). "Environmetric time-series analysis: modelling natural systems from experimental time-series data." International Journal of Biological Macromolecules **13**(3): 190-201.
- Yürekli, K., H. Simsek, et al. (2007). "Simulating climatic variables by using stochastic approach." Building and Environment **42**(10): 3493-3499.
- Yurekli, K. and A. Kurunc (2006). "Simulating agricultural drought periods based on daily rainfall and crop water consumption." Journal of Arid Environments **67**(4): 629-640.
- Zamostny, P., P. Kukula, et al. (1999). "Possible green house gases and global climate change." Chemicke Listy **93**(4): 238-242.
- Zhang, Q. B., G. D. Cheng, et al. (2003). "A 2,326-year tree-ring record of climate variability on the northeastern Qinghai-Tibetan Plateau." Geophysical Research Letters **30**(14): HLS 2-1 HLS 2-4.
- Zhao, L., C.-L. Ping, et al. (2004). "Changes of climate and seasonally frozen ground over the past 30 years in Qinghai-Xizang (Tibetan) Plateau, China." Global and Planetary Change **43**(1-2): 19-31.
- Zuur, A. F. and G. J. Pierce (2004). "Common trends in northeast Atlantic squid time series." Journal of Sea Research **52**(1): 57-72.